Technology Adaptations for Improved Multi-Spectral LIDAR Measurements

Rasmus Grönlund

Diploma Paper

Lund Reports on Atomic Physics, LRAP 296

Lund, February 2003

Abstract

The LIDAR (*LI*ght *D*etection *A*nd *R*anging) technique is in its basic implementation a method to measure the abundance of certain species in the air using laser light, emitted from a source at the same place as where the detection is made. To accomplish this, a powerful light source that is wavelength adjustable is required. Further, LIDAR measurements can be extended to solid targets.

The present work, performed using the existing LIDAR system at the Atomic Physics Division of the Lund Institute of Technology, has focused on three aspects. In LIDAR measurements, precise control of the transmitted wavelength is essential why a wavelength calibration unit is incorporated in a LIDAR system. The calibration unit of the system needed improvements and a new design has been developed to allow facilitated use in wide wavelength ranges. Further, measurements have been performed, aiming at detecting algal growth on high voltage electrical insulators using laser-induced fluorescence. Finally, it was investigated whether LIBS (Laser-Induced Breakdown Spectroscopy) for remote target elemental analysis is possible to accomplish with the system.

Sammanfattning

LIDAR-tekniken (*LI*ght *D*etection *A*nd *R*anging) är i grunden en metod för att mäta förekomsten av vissa ämnen i luften med hjälp av laserljus. Ljuset emitteras från en källa på samma ställe som detektionen görs. För att åstadkomma detta krävs en kraftfull ljuskälla med justerbar våglängd. Vidare kan LIDAR-tekniken utvidgas till fasta mål.

Detta projekt, som har utförts med det befintliga LIDAR-systemet på avdelningen för Atomfysik vid Lunds Tekniska Högskola, har fokuserat på tre aspekter. I LIDAR-mätningar är det viktigt att ha exakt kontroll över den transmitterade våglängden och därför finns en våglängdskalibreringsenhet. Systemets kalibreringsenhet behövde förbättras och en ny design har utvecklats för att erhålla underlättad användning inom ett brett våglångdsområde. Vidare har mätningar utförts för att detektera algbeväxt på högspänningsisolatorer med laser-inducerad fluorescens. Slutligen har en undersökning utförts för att avgöra om det är möjligt att åstadkomma LIBS (Laserinducerad nedbrytningsspektroskopi) med systemet för elementanalys på avlägsna mål.

Contents

1 Introduction

1.1 LIDAR

This project was conducted at the Atomic Physics Division of the Lund Institute of Technology, using the existing LIDAR system operated by the division.

LIDAR is an acronym of *LI*ght *D*etection *A*nd *R*anging (also referred to as laser radar) and is, basically, a method for measuring concentrations of air pollutants in the atmosphere using light. Also, measurements on solid targets can be conducted, for example to study vegetation status or to map algal growth on facades of old buildings.

1.2 Aim of the Thesis

It is important to precisely control the wavelength of the outgoing light when performing LIDAR measurements. Thus, a wavelength calibration unit is incorporated in the LIDAR system. The calibration unit, however, is not designed to work in the entire wavelength span where measurements are made.

The aim of this thesis was to improve and test the existing calibration unit. A further aspect was to demonstrate new techniques for remote solid target characterisation, more specifically to study algal growth on high-voltage insulators in the power grid and to demonstrate elemental analysis of targets using laser-induced breakdown spectroscopy (LIBS). The latter tasks were successfully performed. However, due to problems with delivery of parts it was not possible to finish the calibration unit work on a reasonable time scale, but a complete design of a new unit was accomplished.

1.3 Outline

First, some basic theory is discussed; it is assumed that the reader is familiar with basic atomic physics. In the project, the existing LIDAR system has been used, and since a starting point of this project was to learn as much as possible about it, the system is described next.

After that, a discussion on calibration follows, containing a description of the calibration unit as it is and how it will be improved. Finally, the new types of measurements that were performed on solid targets during the project are described.

2 Theory

2.1 Introduction

In this chapter some theory that is needed to understand the basics of LIDAR measurements is discussed. First, the interaction of matter with light is discussed in Sect. 2.2. Then, Sect. 2.3, covering the theory behind LIDAR and the measurements that can be performed, follows. Finally, a discussion on the theory of an optical parametric oscillator (OPO), the wavelength tuneable laser of the LIDAR system, is found (Sect. 2.4).

2.2 Scattering Processes

2.2.1 Introduction

When light strikes a molecule or particle it interacts with the species in resonance radiation or scattering processes. To be able to make measurements on molecules and particles in the air, scattering processes are essential. The molecules of interest perturb the light and this perturbation can be observed. From these observations, conclusions about the species and its concentration can be drawn. The interaction can occur in a number of different ways, a few of which are described in the following passages. Some different processes are illustrated in Fig. 2.1 [1], [2].

Scattering can be divided into two subgroups, elastic and inelastic scattering. In an elastic scattering process, the scattered wavelength is the same as the exciting wavelength, which is not the case in an inelastic scattering process.

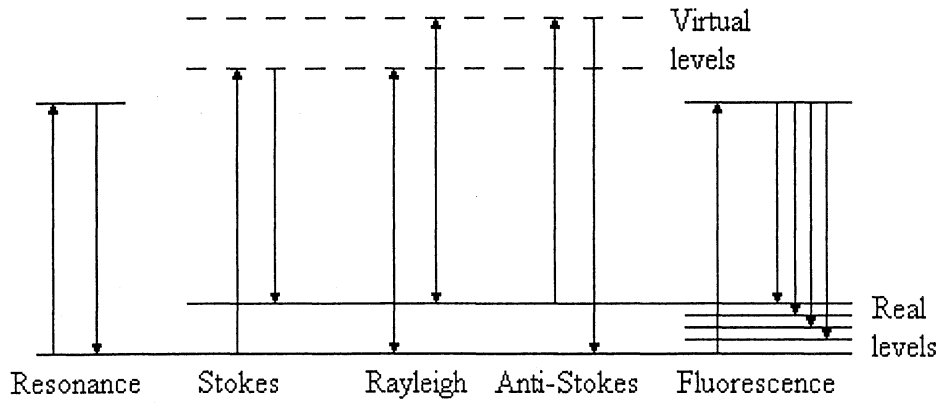

Figure 2.1 - Different light/matter interactions [2].

2.2.2 *Resonance Radiation*

When light of a resonance wavelength strikes an atom or molecule, it can be absorbed and the atom is excited to a higher energy state. Since nature is always striving for having as little energy as possible, the atom will fall back into the ground state (either by stimulated or spontaneous emission) and send out a photon of the same wavelength as the excitation photon. This process is called resonance radiation.

2.2.3 *Rayleigh and Raman Scattering*

When light of a wavelength off the resonance strikes an atom or molecule, the atom can be excited to a virtual energy level. These energy levels are very short-lived (this is defined by the Heisenberg uncertainty principle). When the system returns to the ground level, it emits a photon. However, if the ground level has a substructure, there can be a shift of wavelength as indicated in Fig. 2.1. The elastic scattering is called Rayleigh scattering and the inelastic processes are called either Stokes or Anti-Stokes Raman scattering depending on the wavelength shift [1].

2.2.4 *Fluorescence*

Fluorescence occurs when light excites the atoms/molecules to a high energy state. From this state, the atom can fall down to many different states above the ground state and thus emitting a fluorescence spectrum. Fluorescence occurs principally in solid targets, where the energy levels are "smeared out", which means that the backscattered light will be of a wide distribution of wavelengths.

2.2.5 *Phosphorescence*

Phosphorescence is a phenomenon similar to fluorescence. The atoms are excited to a higher energy state, but from there, for example through collisions, the atoms are de-excited to a state of a different multiplicity, as indicated in Fig. 2.2. This means that the transition back to the ground state is radiatively forbidden, and hence a very long lifetime is obtained. It may be seconds or more before the weak phosphorescence light has ceased to emerge [1].

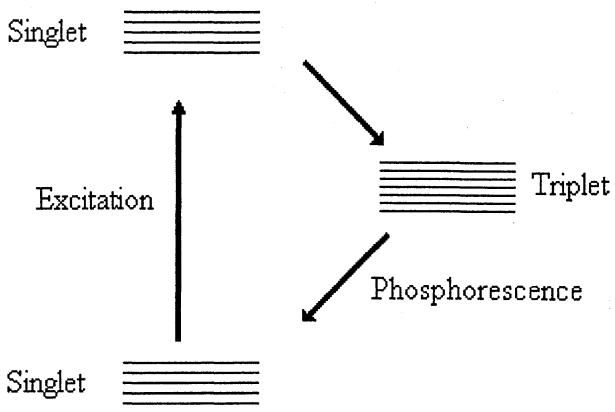

Figure 2.2 - The process of phosphorescence [1].

2.2.6 *Mie Scattering*

Rayleigh scattering, which was discussed in Chap. 2.2.3, occurs when the radiation interacts with molecules, such that the wavelength is much larger than the particles. When the light strikes particles that are considerably larger than the light wavelength, an elastic scattering phenomenon is observed. This scattering is referred to as Mie scattering. Mie scattering is larger for shorter wavelengths and follows an approximate λ^{-2} dependence. Normally, in the atmosphere, Mie scattering from particles is more important than Rayleigh scattering from molecules [1].

2.3 LIDAR Measurements

2.3.1 *LIDAR*

LIDAR is, as previously mentioned, an acronym of *LI*ght *D*etection *A*nd *R*anging (compare: radar - *ra*dio *d*etection *a*nd *r*anging). In the radar case, radio waves are emitted and the backscattered signal from, e.g., aeroplanes or ships is collected. The same is done with LIDAR, but laser light is used instead of radio waves. In this case the backscattered signal comes from molecules and particles in the air, being of sizes in the same order of magnitude as the wavelength. The LIDAR principle is shown in Fig. 2.3.

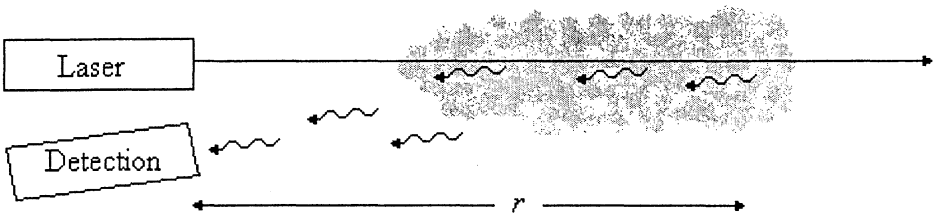

Figure 2.3 - The LIDAR principle. [1]

By measuring the time between the firing of the laser and the detection of the backscattered signal, a range resolved measurement is achieved. The detected intensity backscattered from a distance r at the wavelength λ is given by the general LIDAR equation:

$$P_s(\lambda,r) = DW_p(\lambda)n_b(r)\sigma_b(\lambda)\frac{\Delta r}{r^2}\exp\left(-2\int_0^r \alpha(\lambda,s)ds\right), \tag{2.1}$$

where D is a system constant, W_p is the transmitted pulse energy, n_b is the number density of scatters with the backscattering coefficient σ_b and Δr is the resolution, i.e. the distance between the samplings of the signal. $\alpha(\lambda,s)$ is the volume extinction coefficient, which can be written as

$$\alpha(\lambda,s) = \sigma_m^{Ext}(\lambda)n_m(s) + \int_0^\infty \sigma_a^{Ext}(\lambda,x)n_a(s,x)dx + \sum_i \sigma_i^A(\lambda)C_i(s), \tag{2.2}$$

where the super- and subscripts refer to the extinction (*Ext*) due to scattering by molecules (*m*), aerosols (*a*) with various sizes x, and molecular absorption (*A*) of different compounds with concentration C_i [2].

2.3.2 *DIAL*

DIAL is an acronym of *DI*fferential *A*bsorption *L*IDAR. When trying to find the concentration of a gas in the atmosphere, the LIDAR equation (2.1) contains many coefficients, which causes large uncertainties. Using the DIAL technique, which is illustrated in Fig. 2.4, this problem can be overcome.

The idea is to measure at two different wavelengths, one where the species under study absorbs and another where it does not. At the points where the species exist, the curve measured on the resonance wavelength will be attenuated, and thus there will be a difference between the two curves. This difference is actually what is interesting. Since the wavelengths are chosen close to one another, it is assumed that the only thing that can produce this difference is the presence of the species of interest.

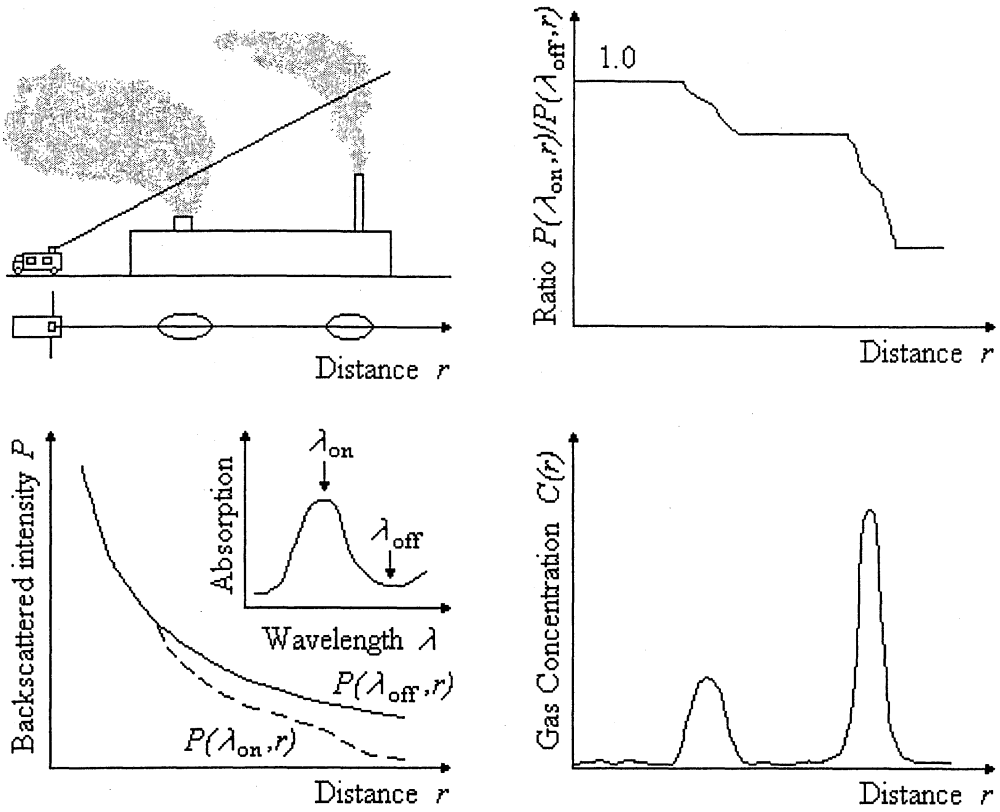

Figure 2.4 - Illustration of the DIAL principle [1].

The upper left part of Fig. 2.4 shows a possible measurement scenario. The laser is shot into the air and through the plumes from a factory (in this example). Below is a top view of the LIDAR truck and the plumes showing where it is expected to get a signal.

Two different wavelengths are transmitted consecutively (every other shot), one wavelength *on* the absorption line and one *off* the absorption line, as close as possible. For a uniform distribution of scatters, both the "on"- and the "off"-curve will follow a general $1/r^2$ dependence (r being the distance from the source), but the "on" wavelength will be attenuated where the measured species exists, see lower left part of Fig. 2.4. The difference in wavelength, however, is considered to be small enough that the Mie scattering can be considered to be the same. Other substances in the atmosphere are also considered to affect both wavelengths in the same way.

With this in mind, the ratio between the "on"-curve and the "off"-curve is calculated. The resulting curve can be described by the equation

$$\frac{P(\lambda_{on},r)}{P(\lambda_{off},r)} = \exp\left(-2(\sigma_{on}-\sigma_{off})\int_0^r C(s)ds\right), \tag{2.3}$$

and is illustrated in the upper right part of Fig. 2.4. Eq. (2.3) can be rewritten as

$$C(r) = \frac{d}{dr}\left(\frac{1}{2\Delta\sigma}\ln\frac{P(\lambda_{on},r)}{P(\lambda_{off},r)}\right), \tag{2.4}$$

which gives us the concentration as a function of r. The final curve that is achieved will have an appearance like the lower right part of Fig. 2.4 [2].

By shooting the laser in different directions, a two-dimensional concentration map can be achieved. When measuring through a plume from a factory, the total flux emitted from the factory is interesting. Then the concentration map can be integrated over the area to give a total concentration in the somewhat strange unit kg/m. If the measured value is multiplied by the wind speed perpendicular to the measurement direction, the flux is given in kg/s.

2.3.3 *Fluorescence LIDAR*

In many applications the fluorescence from far away objects is an interesting topic to study. Examples of such applications may be investigation of algal growth and stone degradation in old buildings [3], [4] or classification of different materials in an object [2]. The fluorescence process is briefly described in Sect. 2.2.4, and visualised in Fig. 2.1.

The laser is shot at a target and fluorescence is induced (LIF - Laser Induced Fluorescence). The fluorescence is scattered in all directions and a small amount of the light is scattered back towards the telescope. The incoming light is analysed and a fluorescence spectrum is attained.

It may be interesting to be able to focus the laser onto a contaminated point and thereby burn the contamination off the studied area. Since the fluorescence can be measured slightly before, almost simultaneous control and cleaning could be achieved. However, this is not a reality so far, but in a not too distant future it could be.

2.3.4 *LIBS*

LIBS is an acronym for *L*aser *I*nduced *B*reakdown *S*pectroscopy and is also referred to as LIPS (*L*aser *I*nduced *P*lasma *S*pectroscopy). In this method, a powerful laser beam is focused onto a solid target. If the intensity in this point is large enough, a laser-induced plasma is produced. In the plasma, all chemical bonds are broken and many of the elements are ionised. Thus, this plasma emits characteristic lines of the material under examination. Immediately after excitation, the backscattered radiation will be dominated by intense broad-band radiation, but after a little while (about 1 μs), the characteristic lines of the studied material appear [5], [6].

2.4 Optical Parametric Oscillator

2.4.1 *Introduction*

An Optical Parametric Oscillator (OPO) is a device for the generation of tuneable laser radiation, which, of course, is very useful for LIDAR measurements. It uses an all-solid-state configuration to achieve the wavelength tunability, in contrast to the dye laser arrangement, which is commonly used in LIDAR applications. For a dye laser, several different dyes are needed to be able to scan the entire visible spectrum, which is not only inconvenient while using them; it also inhibits fast tunability other than in very small wavelength intervals. In an OPO all these wavelengths can be produced by changing only angles of crystals and mirrors [7].

2.4.2 *Non-linear Processes*

The OPO uses non-linear processes in a crystal to achieve laser tuning. Different kinds of non-linear processes exist, such as frequency doubling, sum frequency generation or difference frequency generation. In these processes, sums and differences of two incoming photons generates a single output photon.

The non-linear process used in an OPO is visualised in Fig. 2.5. In this process, a single photon is split into two photons with lower frequency. The incoming beam is called a *pump* beam and the produced light is referred to as a *signal* and an *idler* beam. For the process, the conservation of energy gives that

$$\omega_p = \omega_s + \omega_i, \tag{2.5}$$

where the indices p, s and i denote pump, signal and idler, respectively. Eq. (2.5) can also be expressed using wavelengths,

$$\frac{1}{\lambda_p} = \frac{1}{\lambda_s} + \frac{1}{\lambda_i}. \tag{2.6}$$

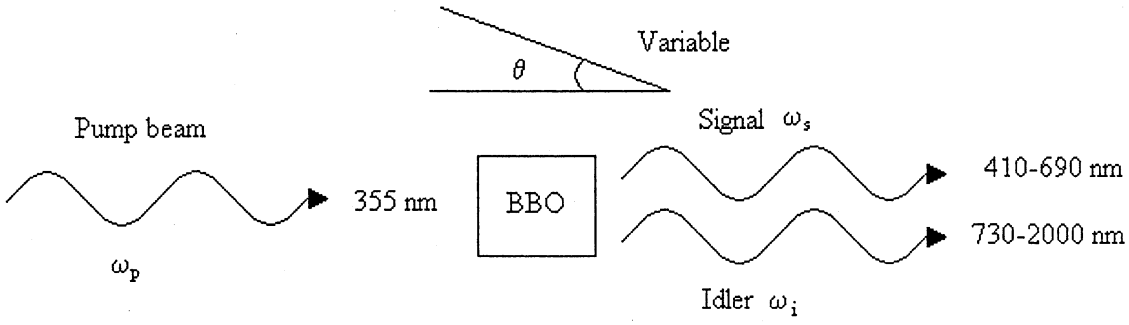

Figure 2.5 - The non-linear process in an OPO [7].

2.4.3 *Phase Matching*

In order to get any gain in the non-linear crystal, the process must be phase-matched. This is because there must be conservation of momentum in the process. The k-vector (or wave vector) is a vector representing the direction and frequency of a light wave. The frequency is given by the length of the k-vector, and the direction of the wave is given by the direction of the k-vector. The conservation of momentum can then be expressed as

$$\mathbf{k}_p = \mathbf{k}_s + \mathbf{k}_i, \tag{2.7}$$

where the indices again represent *p*ump, *s*ignal and *i*dler, respectively.

There are two different types of phase matching, collinear and non-collinear. In the case of collinear phase matching the k-vectors are parallel, which is not the case for non-collinear phase matching, as can be seen in Fig. 2.6.

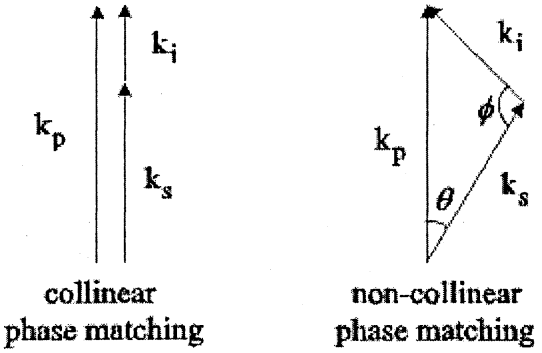

Figure 2.6 - Collinear and non-collinear phase matching [7].

Since $k = n \cdot \omega$, k being the length of vector **k**, Eq. (2.7) can, in the case of collinear phase matching, be rewritten as

$$n_p\omega_p = n_s\omega_s + n_i\omega_i, \tag{2.8}$$

where n_x is the refractive index for the respective waves.

In uniaxial crystals (that are being considered in this case), the refractive indices are different for different directions through the crystal, or more specifically, n is a function of the angle between the optic axis of the crystal and the k-vector, $n = n(\theta)$. Thus, turning the crystal makes it possible to fulfil Eq. (2.8) for all wavelengths in the desired span [8].

If non-collinear phase matching is achieved, the angle between the pump beam and the signal will be constant, but as the frequency is tuned the length of the signal k-vector will change. Since the phase matching must be preserved, the length of the signal beam as well as the angle ϕ will change, which means that the idler beam will diverge from the optic axis of the cavity as the frequency is tuned [7].

3 The Lund LIDAR System

3.1 Introduction

In this chapter the Lund LIDAR system is briefly described. The chapter first gives an overview (Sect. 3.2), and then the laser system (Sect. 3.3), the transmitter and receiver (Sect. 3.4) and the computer system (Sect. 3.5) are presented.

3.2 Overview

The LIDAR technique has been used in Lund for more than 20 years, during which systems have been changed and rebuilt several times. During recent years, the dye lasers have been exchanged for an OPO system. The computer programs have also been developed recently.

The current LIDAR system of the Atomic Physics Division of the Lund Institute of Technology is based on a Volvo F610 truck. This makes the system mobile, which creates the possibility to perform measurements wherever needed. An overview of the system is seen in Fig. 3.1.

The LIDAR truck is equipped with an air-conditioning system, because the OPO system is very sensitive to temperature changes. Thus it is important to keep a constant temperature inside the truck at all times. The system is capable of keeping the temperature within ±2°C in the outside temperature interval of -20°C to +30°C.

The entire system is thoroughly described in [9].

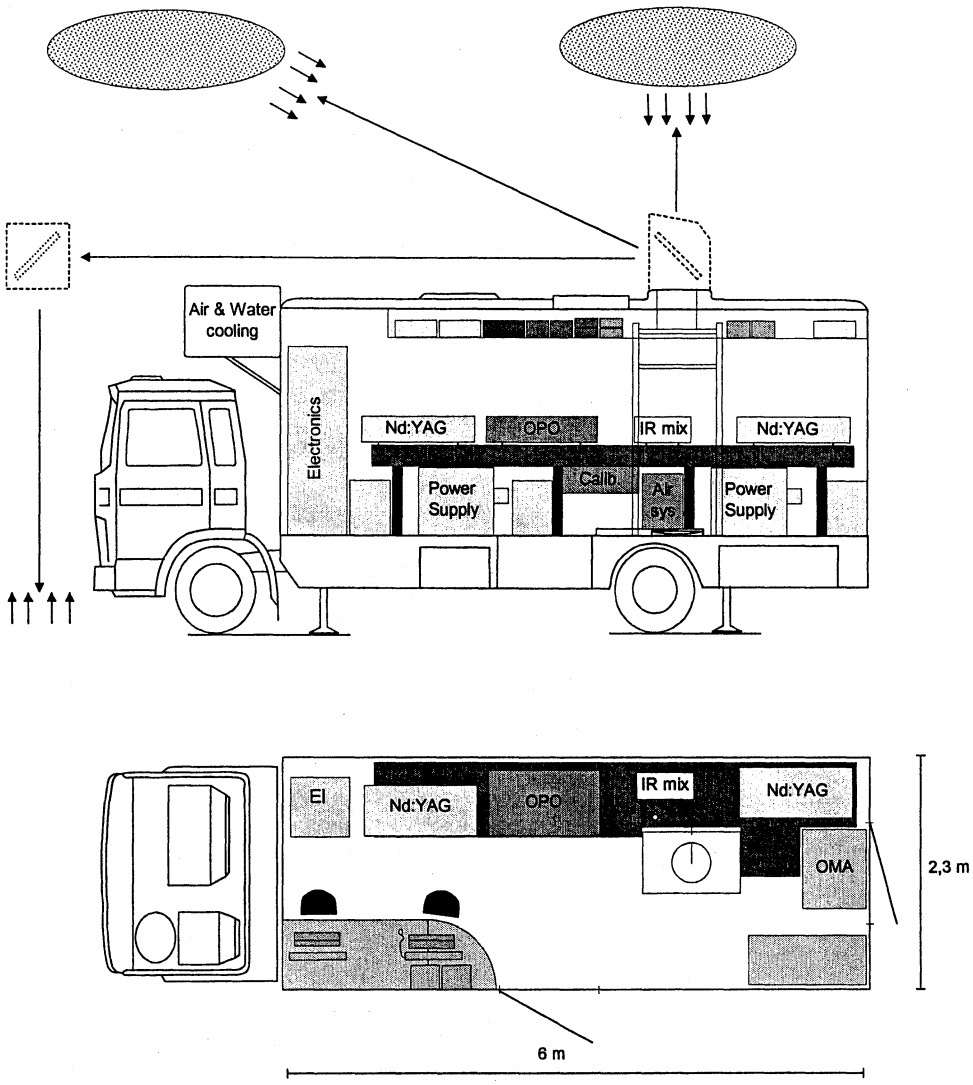

Figure 3.1 - Overview of the Lund LIDAR system [9].

3.3 Laser System

The laser system in the LIDAR truck is built up of four different units, two Nd:YAG lasers, one Optical Parametric Oscillator (OPO) and one IR-mixing unit. Together these units can be adjusted to produce laser light in the wavelength spans 220-690 nm, 730-1800 nm and 2600-4300 nm, thus constituting an extremely versatile system that can be used in a variety of different applications [10].

3.3.2 Nd:YAG Laser

The Nd:YAG laser is a very commonly used laser, employing neodymium doped yttrium aluminium garnet crystals. It operates in a pulsed mode on the fundamental wavelength 1064 nm, but can with high efficiency be frequency converted to the double (532 nm), the triple (355 nm) and even the quadrupled (266 nm) frequency. To get intense radiation from the laser, it is Q-switched, which means that the laser beam is inhibited until a

maximal inverted population is achieved. This gives a short (<10 ns), very intense pulse (tens of MW) [11].

The system is pumped by two Nd:YAG lasers. Nd:YAG 1 is pumping the OPO unit and is running on the tripled frequency (355 nm). Nd:YAG 2 is pumping the IR-mixing unit and is running on the fundamental frequency (1064 nm). The entire system is running at a 20 Hz repetition rate and an advanced trigger system is used to ensure that the pulses are synchronised.

3.3.3 *OPO Unit*

The theory of the OPO unit was discussed in further detail in Sect. 2.4.

The OPO of the LIDAR system in Lund is a modified Quanta-Ray MOPO-730. It is divided into two parts, one Master Oscillator (MO) and one Power Oscillator (PO). The Master Oscillator is used to choose the correct wavelength while the Power Oscillator amplifies the signal.

The BBO (β-Barium Borate) crystal of the Master Oscillator is placed in a cavity as shown in Fig. 3.2. Photons of all possible wavelength pairs are created in the BBO crystal by quantum noise fluctuations, but the diffraction grating and the tuning mirror are positioned to pick out one particular wavelength, the desired signal wavelength. Now the crystal will be seeded by these photons and hence this wavelength will be strengthened.

To improve the efficiency, the pump beam out is reflected back into the cavity where it is used to enhance the signal in the backward direction through the BBO crystal.

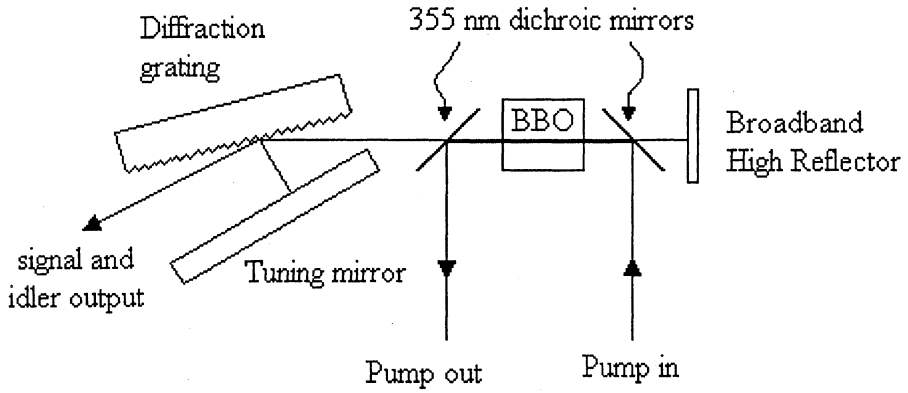

Figure 3.2 - The cavity of the Master Oscillator [7].

The output from the Master Oscillator is the zeroth order reflection from the grating while the first order reflection is directed back into the cavity to increase the strength of the output light [7].

The output is transferred to the Power Oscillator part of the OPO where it is mixed with a 355-nm pump beam. The Power Oscillator is actually an OPA (Optical Parametric Amplifier) which is a BBO crystal in an unstable cavity, see Fig. 3.3, resulting in only one passage through the BBO crystal. In this

process the Master Oscillator output is amplified to give greater output effect.

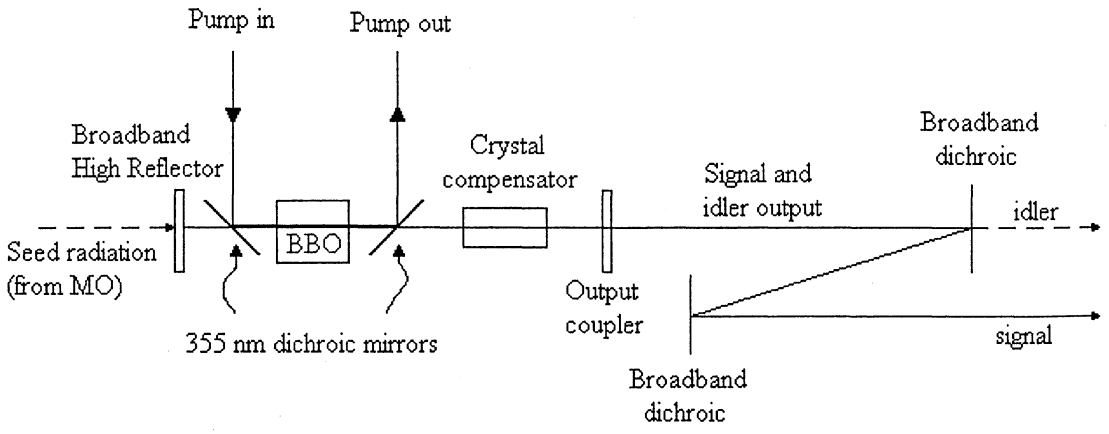

Figure 3.3 - The Power Oscillator part of the Quanta Ray MOPO-730 [7].

The output from the Power Oscillator is one signal beam and one idler beam. The signal is in the wavelength span 440-690 nm and the idler beam will give (less powerful) radiation in the wavelength region 730-1800 nm. By using the frequency doubling crystals laser radiation can also be produced in the wavelength span 220-440 nm. [10].

The MOPO is modified, by a few built in piezo-electric elements that enable fast wavelength tuning, without having to turn any motors. Instead, a voltage may be put over a piezo-electric element, and thus the frequency may be precisely tuned to a certain wavelength. As long as the wavelength difference is small enough to make it possible to tune the wavelength using only the piezo-electric elements, the frequency can be changed on a shot-to-shot basis (within 50 ms).

3.3.4 IR-mixing Unit

The infrared mixing (IR-mixing) unit is similar in its configuration to the OPO unit, in that it uses two Lithium Niobate ($LiNbO_3$) crystals to mix the idler output from the OPO with 1064 nm laser light from Nd:YAG 2. The non-linear process in the crystals will then be a difference frequency generation to obtain wavelengths in the infrared region. By choosing appropriate idler wavelengths from the OPO unit and choosing correct angles of the crystals, laser light in the wavelength span 2600-4300 nm can be produced [10].

3.4 Transmitter and Receiver

The laser light is transmitted into the atmosphere through the dome, which is hoisted to the roof of the LIDAR truck. In the dome, a beam expander is used to increase the size of the beam. The transmitter and receiver are illustrated in Fig. 3.4. The dome can be rotated 360 degrees and a folding

mirror inside the dome can be tilted to transmit the light beam in a vertical angle between -10 and 55 degrees.

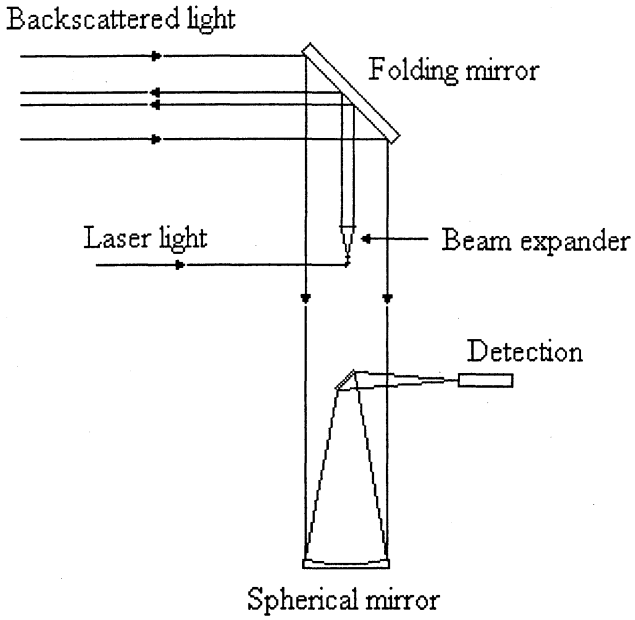

Figure 3.4 - Transmitter and receiver system [2].

The dome also collects the backscattered light and directs it to a large spherical mirror on the floor of the truck. In this way all the light that is collected by the dome is projected onto a small point. When performing DIAL measurements, a narrow-band filter is placed in front of a photomultiplier tube (PMT) to record only elastically backscattered light and to suppress background radiation.

In fluorescence measurements another type of filter is placed in front of the detection. The filter is designed to block the exciting wavelength, which would otherwise give a very strong signal. In the point where the light is projected, the end of a fibre connected to an optical multichannel analyser (OMA) system is placed to give the full spectrum.

3.4.1 *Optical Multichannel Analyser*

An optical multichannel analyser is often referred to as an OMA system, or a fluorosensor [12]. It is a device constructed to analyse the spectral contents of incoming light. It mainly consists of a spectrometer that separates the different wavelengths in space and projects the light onto a Charged Coupled Device (CCD) camera. The intensity of light onto a column of the CCD camera will be a measure of how much light there is in a certain wavelength span. The resolution is limited by the number of pixels of the CCD camera and the width of the entrance slit.

An overview of the OMA system that has been used in this project is shown in Fig. 3.5. The lasers in the right part of the figure can be used to emit exciting light through the fibre. In the case of the studies made in this

project, however, this light is not sufficiently intense to get results, so the system has only been used to analyse the incoming light.

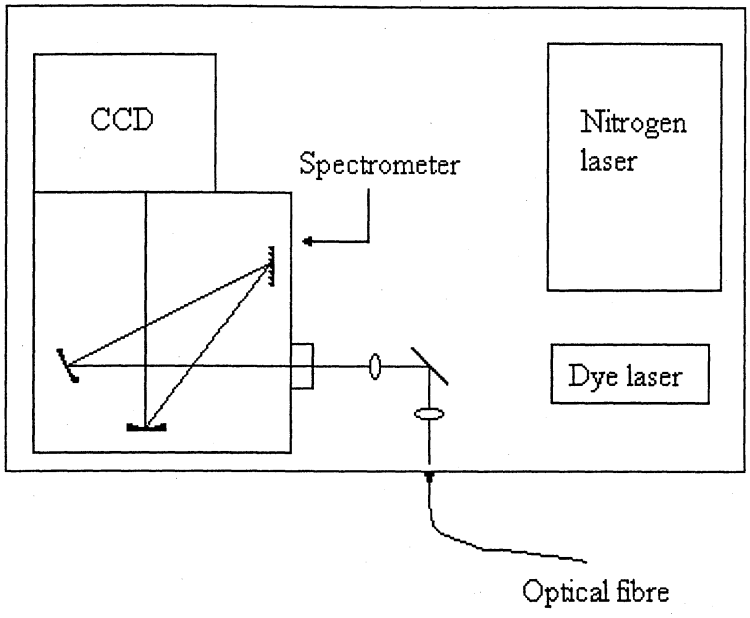

Figure 3.5 - The OMA system used in the project.

When using the OMA system for measurements of fluorescence, the incoming light that is desired to be measured is a short pulse. This pulse would be drenched in the background if the average light was measured. To overcome this problem, the CCD can be time-gated, which means that it only measures for a short time (≤100 ns). Since we know when the fluorescence pulse is supposed to come (assuming we know the distance to the target) we can set a proper delay to make sure that the CCD measures at the correct time, capturing the full laser-induced signal but only a fraction of the background light. The CCD also incorporates an image intensifier, which strengthens the signal, to make it possible to measure small intensities.

3.5 Computer System

3.5.1 Overview

The entire system is controlled by four computers in a network system. The computer software controls everything from dome steering to OPO wavelength calibration. The software of the system is developed using the graphical programming language LabView, provided by National Instruments Corporation.

3.5.2 LabView

LabView is a program development tool where the programs are built up in block diagrams. The block diagrams are developed with the programming

language G, in which the source code is "drawn" instead of being written as in ordinary text-based programming languages. Each program in LabView is called a Virtual Instrument (VI), consisting of a front panel and a data flow diagram. The front panel is the part that is seen by the user of the program where data is entered and results displayed, whereas the data flow diagram (or block diagram) is the actual source code [13]. An example of the appearance of a front panel is seen in Fig. 3.6 and the corresponding block diagram is found in Fig. 3.7.

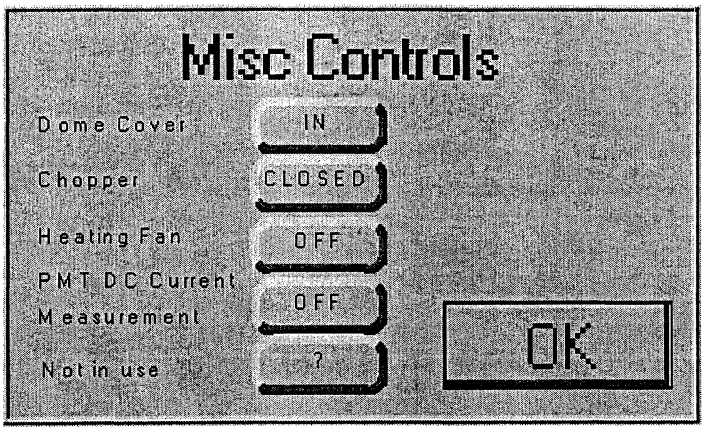

Figure 3.6 - An example of a VI front panel.

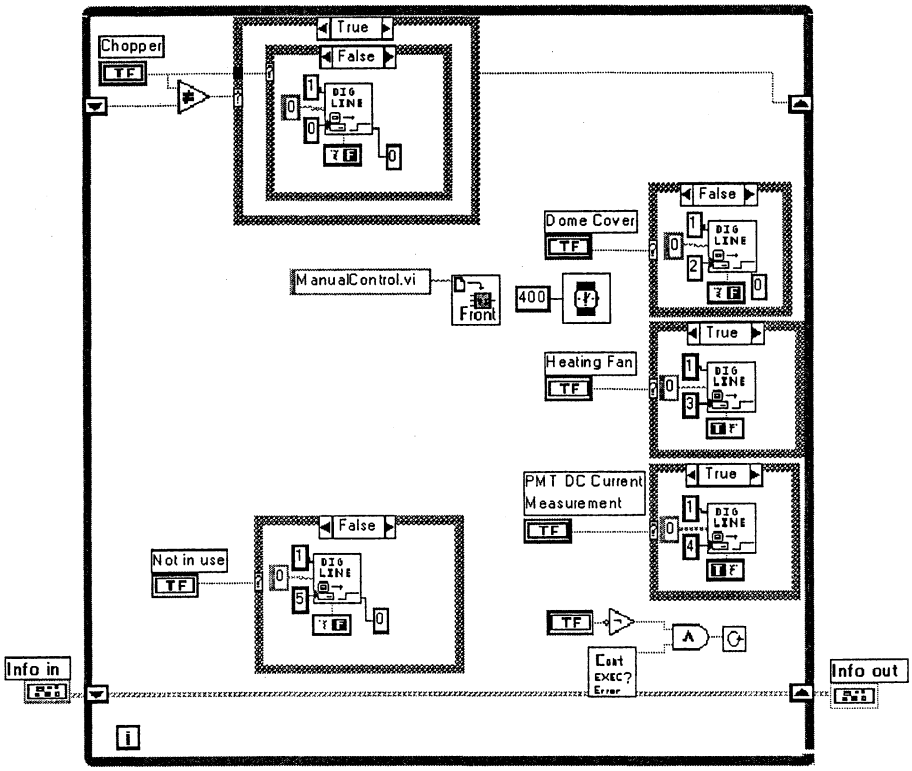

Figure 3.7 - The block diagram corresponding to the front panel in Fig. 3.6.

4 Calibration

4.1 Introduction

When performing LIDAR measurements, it is essential to be sure that the correct wavelengths are used. If the wavelength drifts, which may happen for a number of reasons, it is highly desirable with an automatic calibration routine for the OPO unit to guarantee that the correct wavelengths are used at all times. In this chapter, the original design is briefly discussed and then the new design is presented.

4.2 Original Calibration Unit

4.2.1 Original design

The task of the calibration unit is to check the wavelength of the system. This is done using a gas cell system. A diffuse reflex (4%) of the laser light is directed into the unit and through a neutral density filter, as seen in Fig. 4.1. There are a number of filters, mounted on a wheel, so that an appropriate damping can be accomplished. The laser beam is then split into two optical paths, one passing through an absorption cell onto a detector and the other going directly onto a detector.

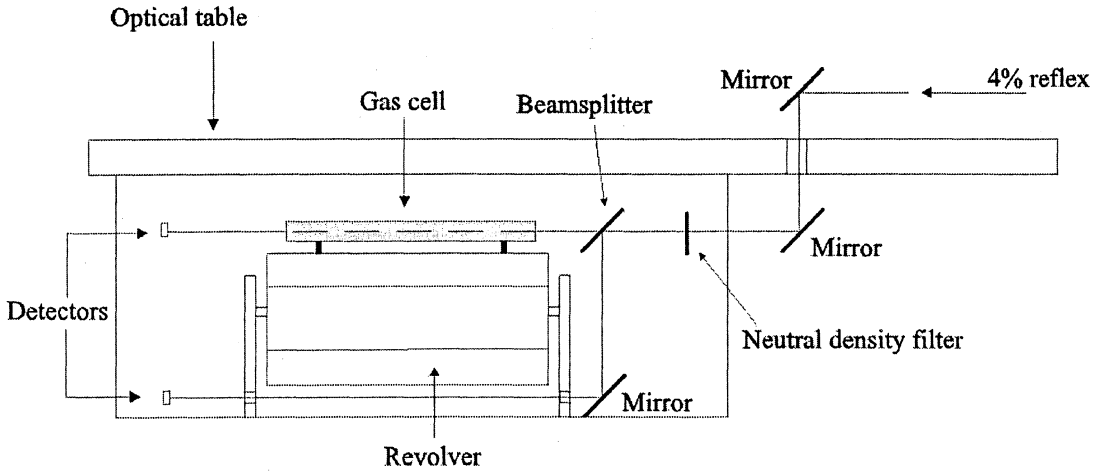

Figure 4.1 - The original layout of the calibration unit [14].

The signals from the two detectors are divided to suppress fluctuations in the laser intensity etc. The wavelength is swept to find the point of absorption of the gas. In this way the laser is calibrated according to the gas, so that it is known that the wavelength used in the measurement is the correct one.

The original layout is completely described in [14].

4.2.2 *Problems*

At the start of the current work, the calibration unit did not work as desired. There were a number of problems that needed to be attended to.

- The calibration unit was only designed to work in the wavelength span 190-1150 nm, since the detectors only worked in this wavelength region. However, the detectors are mounted on a wheel, making it possible to easily install more detectors.
- The damping of the incoming laser light was not satisfactory. The wheel containing the neutral density filters did not contain a large enough number of filters. This means that more filters have to be put in the beam path manually.
- The beamsplitter was not a perfect 50-50 beamsplitter, so the beam passing through the gas cell had to pass through additional neutral density filters. Also, the beamsplitter did not work in the entire wavelength span of the OPO unit.
- Adjustments needed to be done since the beam passing through the gas cell also passed through two windows. This was solved by placing an empty cell in the path of the reference beam, but this was not accounted for in the original design.
- The alignment was cumbersome.
- No good calibration routine was implemented and calibration when measuring on hydrocarbons, with many different absorption peaks, needed to be implemented.

The idea was to solve all these problems and to implement an automatic calibration routine.

4.3 Design

4.3.1 *Introduction*

At the beginning of this project, the idea was to make the needed adjustments to the calibration unit and to make a full implementation and test of the functionality. However, this has not been possible, due to long delivery times of some components needed. A full design of the new unit has been done, which is presented in this chapter.

4.3.2 *Overview*

The suggested design is to use optical fibres to overcome the cumbersome alignment of the unit and it also offers an efficient solution of the damping problem. A sketch of the design is shown in Fig. 4.2.

The diffuse reflex is directed into a fibre connection box (Sect. 4.3.4), where it is coupled into four optical fibres, two transmitting in the UV-Visible area and two transmitting in Visible-IR (Sect. 4.3.3). On the way to the calibration unit, there is a damping stage (Sect. 4.3.5) and in the unit, the

light is collimated using off-axis parabolic mirrors (Sect. 4.3.6). Finally, one path of the light is directed through the gas cell and the reference beam is directed directly onto a detector (Sect. 4.3.7).

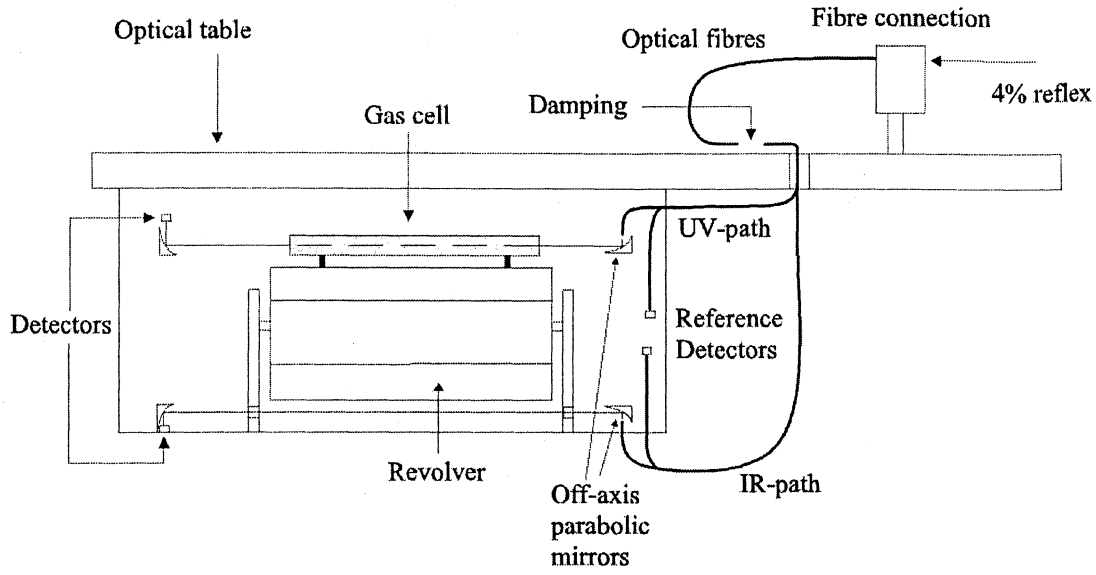

Figure 4.2 - The suggested new design of the calibration unit.

4.3.3 *Optical Fibres*

The idea of the new design of the calibration unit is to lead the light into the unit using optical fibres. It seems it is not possible to find fibres transmitting light in the entire wavelength region, so two different types of fibres will be used.

Much effort was put into finding fibres that could be suitable, but finally the fibres FG-200-UCR (transmitting from 200 nm to 1100 nm) and SG-FF-180 (transmitting from 500 nm to 4.0 μm) from Thorlabs Inc. were chosen [15].

Other possible fibres would have been a HPSUV series and a CHAL series fibre from Oxford Electronics Ltd. transmitting in the wavelength span 180 to 1200 nm and 1 to 6 μm respectively. Oriel Instruments also supply a possible IR fibre, transmitting in the wavelength span of 600 nm to 4.5 μm.

4.3.4 *Fibre Connection*

The incoming laser light must be guided into the fibres to make it possible to make the measurements. The laser beam is guided onto an off-axis parabolic mirror (A8037-101 from Janos Technology Inc.) and onto a rough surface. This is because the beam has to be equally divided between four fibres sitting close together. Since the mode pattern of the laser beam can change on a shot-to-shot basis, the intensity would not be equally divided and especially not controlled if the beam simply was directed onto the fibre ends. The rough surface, however, scrambles the mode and the diffuse reflex from it will be equally picked up by the four fibre ends.

Another idea is to guide the beam through a thin slice of white scattering ceramic, e.g. Al_2O_3, which would also scramble the mode of the laser light

and make it equally divided into the fibres. However, it has not been examined how much light is needed into the fibres, therefore it has not been decided which method to use. Most likely is that both options will be available, since the laser light can vary in intensity over the wavelength interval. The design of the fibre connection box is shown in Fig. 4.3.

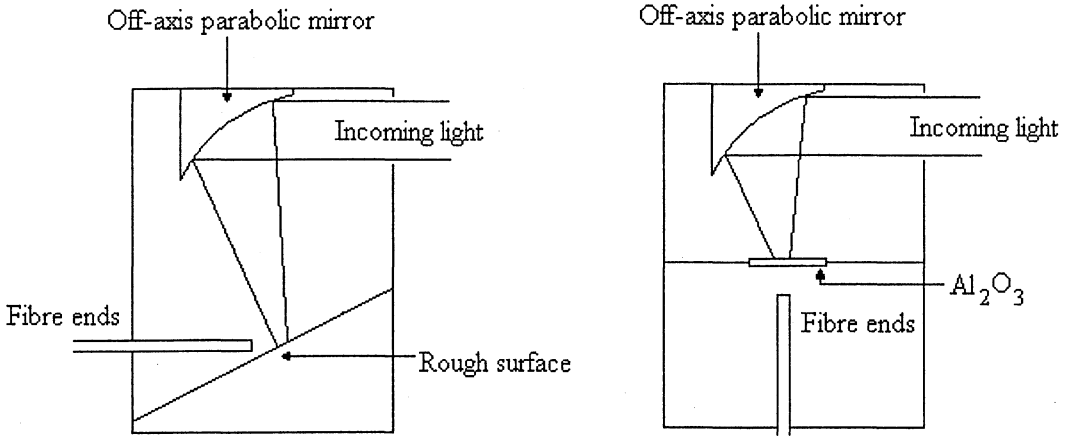

Figure 4.3 - Top view of the fibre connection box for two possible designs.

The reason why an off-axis parabolic mirror, (explained in more detail in Sect. 4.3.6), is used in the fibre connection box is because it is not known what intensity of light will be needed into the fibres. Therefore it is convenient to be able to pass the light through a focus, giving the possibility of very large intensities into the fibres.

4.3.5 *Damping*

The damping problem can be solved in a clever manner when using optical fibres. By putting two fibre ends close to one another such that the separation between them can be adjusted, damping can be accomplished. The degree of damping can easily be regulated by moving the fibre ends. This is done separately for the reference and the cell beam, so that the amount of light hitting the detectors can be adjusted to be the same for both optical paths.

An experiment has been performed to explore damping of light in this manner. The experiment was done using 60-μm diameter optical fibres and a continuous HeNe laser. In the calibration unit, larger diameter fibres will be used, which means that it will be easier to get light through the fibres. The experiment proved that the signal transmitted over the gap between the fibres was extremely sensitive to sidewise movements of the fibres. The set-up of the experiment is seen in Fig. 4.4.

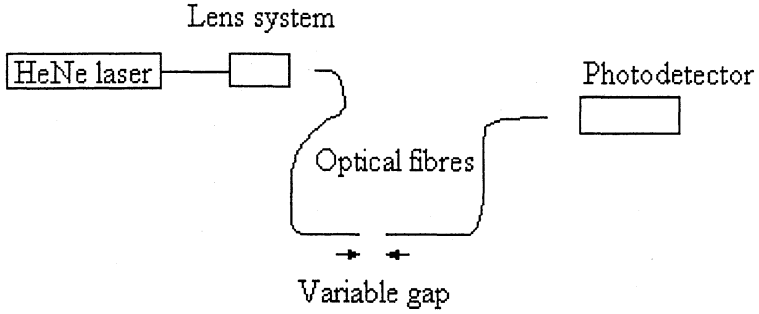

Figure 4.4 - Set-up of experiment.

The result of the experiment is seen in Fig. 4.5. It can be seen that damping can be achieved and adjusted. Unfortunately, it was not possible to measure the exact distance between the fibres, but the equipment was designed such that equal steps could be achieved. Also, the maximum signal could not be found, since the fibre ends are sensitive and therefore it was not possible to get them closer together using the available equipment. However, without the damping stage (i.e. the transmission through one fibre only) a signal of 2.5 V was measured.

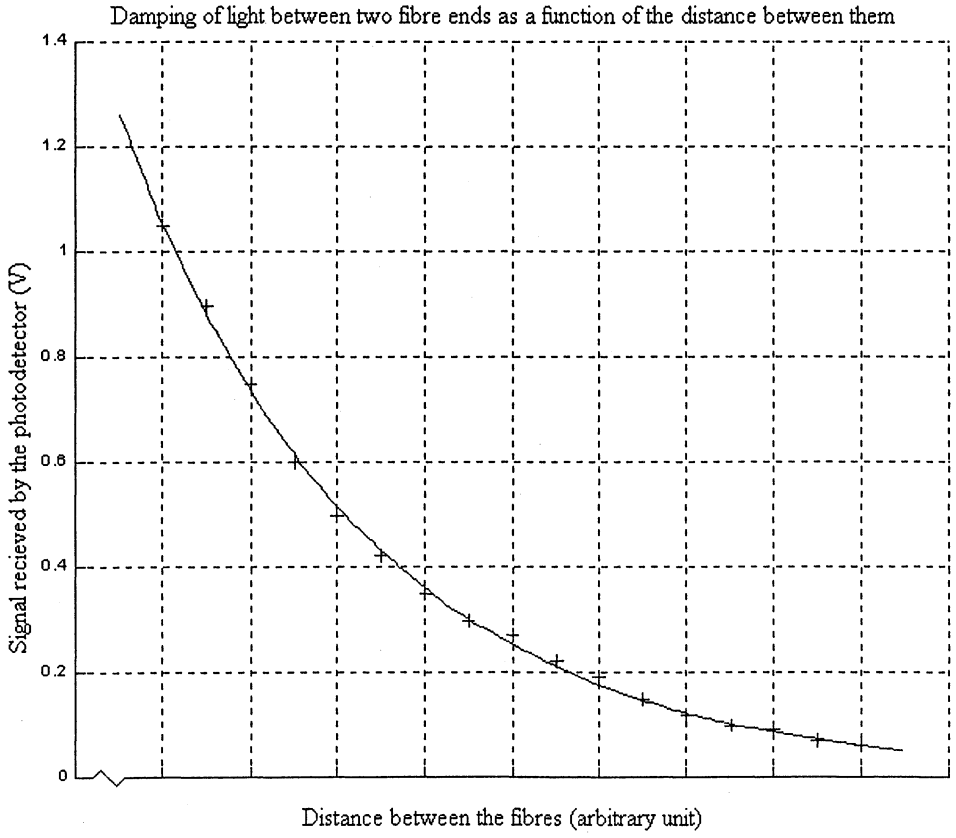

Figure 4.5 - Damping between two fibre ends as a function of the distance between them.

An exponential line has been fitted to the measured points and it seems to interpolate the data well.

4.3.6 *Off-axis Parabolic Mirrors*

When using fibres, the light is emitted from a fibre end at an angle determined by the numerical aperture (NA) of the fibre. The numerical aperture of a fibre is defined as $NA = \sin\theta$ where θ is defined as in Fig. 4.6.

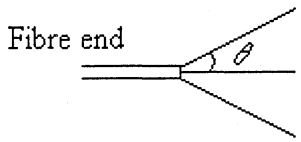

Figure 4.6 - Definition of numerical aperture.

To be able to send the light through the gas cell, the light has to be collimated. Ordinarily, collimation is accomplished using lenses, but in this case too large a wavelength span is considered to make lenses an option. The solution chosen to this problem was to use off-axis parabolic mirrors that can collimate light of many different wavelengths, see Fig. 4.7. The only limiting factor on what wavelengths can be collimated is the reflectance of the material.

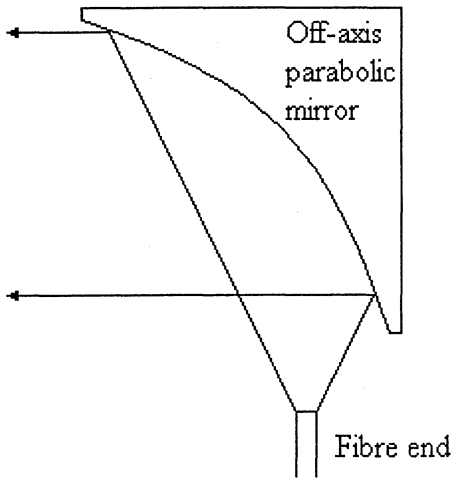

Figure 4.7 - Off-axis parabolic mirror used to collimate light from an optical fibre.

The off-axis parabolic mirrors that are to be used were delivered by Janos Technology Inc. and are coated with aluminium, which has more than 90 % reflectance in the entire desired wavelength span. The mirrors chosen were A8037-175, since these mirrors have an appropriate focal length and size to match the NA of the chosen fibres.

4.3.7 *Optical Paths*

Since we are using two different fibres and, more importantly in this case, two different detectors, it is needed to divide the light into different optical paths to make the measurements. The incoming laser light is coupled into the fibres (see Sect. 4.3.4) and then directed into the calibration unit. Since different detectors are to be used, there has to be one optical path for the UV-Visible light and one for the Visible-IR light.

The idea is to set up the fibre ends and off-axis parabolic mirrors once and for all, not having to perform any alignment in the calibration unit after installation. Since the gas cells are placed on a revolver, the optical paths do not have to be in the same places as in the original layout.

4.3.8 *Programming*

An automatic calibration routine has been implemented, adjusting a Gaussian profile curve to four measured values and finding the peak of the curve. It is assumed that the wavelength has not drifted more than making it possible to find the peak in this manner. The routine has been implemented, but is yet to be incorporated into the system.

5 LIDAR measurements

5.1 Introduction

Within the scope of this project, some LIDAR measurements have been performed. The measurements that have been performed were fluorescence measurements (Sect. 5.3) and LIBS measurements (Sect. 5.4). For reasons of completeness, a short passage on DIAL measurements is also included (Sect. 5.2), with references to measurements that have previously been performed using the LIDAR system.

5.2 DIAL

The Lund LIDAR system has previously been used to perform measurements using the DIAL technique, aiming at finding the concentration of different substances in the atmosphere. Examples of such campaigns can be found in [16] (industrial SO_2 flux measurements), [17], [18] (volcanic SO_2 emission) and [19] (mercury emission from a chlor-alkali plant).

5.3 Laser Induced Fluorescence

5.3.1 Introduction

As discussed in Sect. 2.3.3, typical laser induced fluorescence (LIF) measurements that previously have been performed are aiming at finding algal growth on buildings or other objects [3], [4]. This is quite easily performed since algae has a sharp peak at ~690 nm from chlorophyll. Using multivariate analysis (see Sect. 5.3.3), more subtle differences in spectra can be found, which makes it possible to e.g. distinguish objects of different materials from each other [2].

5.3.2 Measurements

The images in this chapter are taken from measurements on electrical insulators that were made during the course of this project. Earlier measurements have been performed in order to examine whether algal growth on insulators affect their performance and the purpose of the present study was to perform measurements for algae detection in a situation similar to real-life.

The fluorescence was induced on the insulator using the frequency-tripled radiation of one of the LIDAR Nd:YAG lasers, operating at a wavelength of 355 nm with a repetition rate of 20 Hz and a pulse duration of 4-5 ns. The mean power was about 0.5 W, which yields a pulse energy of around 25 mJ. The laser beam is sent through the transmitter (which is discussed in Sect.

3.4), where the beam diameter is increased from 5 mm to 3 cm. The beam is transmitted towards the insulator, which is placed ~60 m from the laser source, and fluorescence is induced in the material.

Backscattered light is collected by an optical multichannel analyser (OMA), which was described in Sect. 3.4.1. The OMA system records the full spectrum of the incoming light. The small pulses of fluorescence light, however, are much smaller than the background light on a time average. To suppress this problem, the OMA system is time-gated, so that it only registers light at the time that is of interest, which is known if the distance to the target is known. In a short, properly centred, time interval (100 ns), the interesting signal is considerably larger than the background signal and interesting information can be extracted. The signal was averaged over 20 shots to achieve a better signal to noise ratio.

A typical spectrum from a point on an insulator with algal growth is seen in Fig. 5.1. Note the massive fluorescence peak from chlorophyll at ~690 nm. For comparison, a spectrum from a clean part of the insulator is shown in Fig. 5.2.

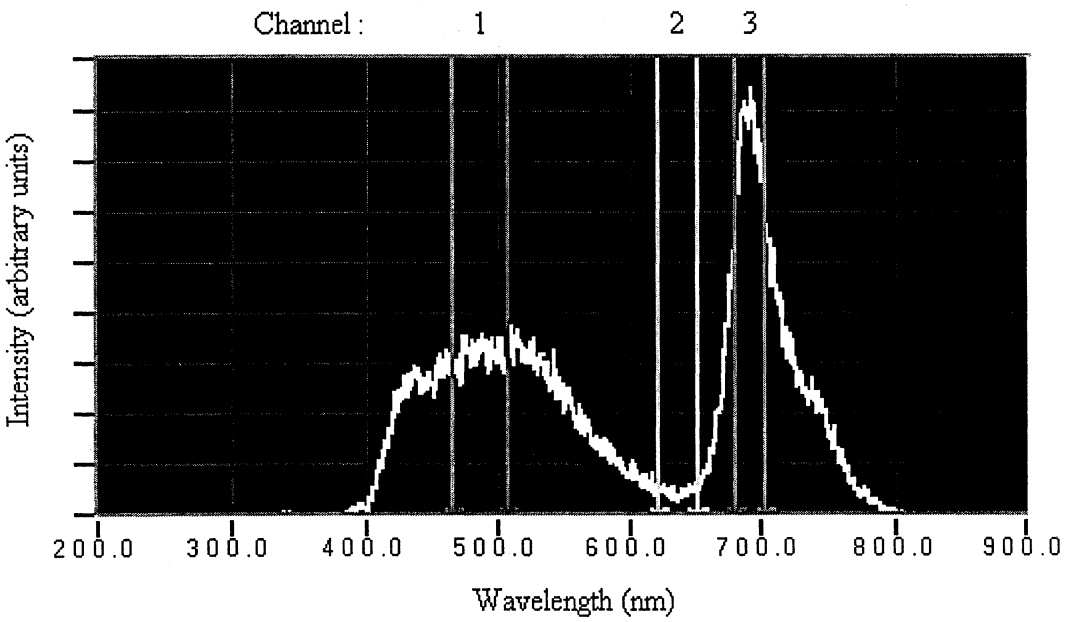

Figure 5.1 - A typical fluorescence spectrum from an insulator area covered by algae.

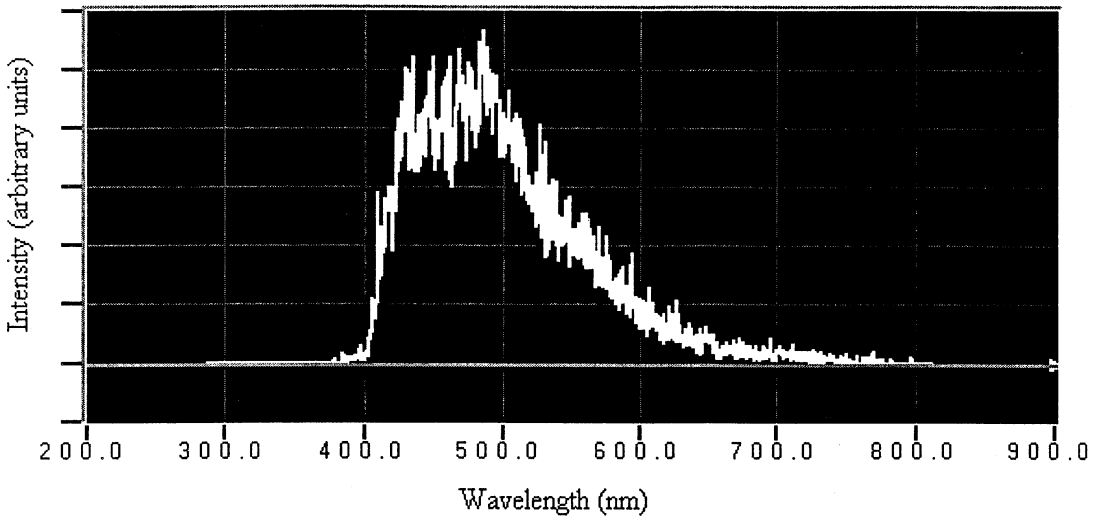

Figure 5.2 - Fluorescence spectrum from a clean part of an insulator.

By sweeping the laser over the object that is to be studied, the spectrum in each point can be recorded. This is a good example of multi-spectral imaging [20]. As described in Sect. 3.4, the dome can be rotated 360 degrees and the mirror can be tilted from -10 to +55 degrees, with a horizontal resolution of 0.0035 degrees and a vertical resolution of 0.011 degrees. Since the insulator is placed at a distance of ~60 m from the laser source, the angular resolution corresponds to a horizontal and vertical resolution on the insulator of 3.7 mm and 12 mm, respectively.

In Fig. 5.1, the vertical lines mark different wavelength bands. By evaluating a cleverly selected function of the mean values in the channels, different properties of the spectrum can be enhanced. In this case, where it is of interest to find all points with algal growth, a good function would be:

$$\frac{\text{Channel 3} - \text{Channel 2}}{\text{Channel 1}}, \tag{5.1}$$

where the channels are defined as in Fig. 5.1.

In this way, only the points containing a large peak at 690 nm will give a large value. The same function for the point shown in Fig. 5.2 will give a value close to or even below 0, since channel 3 and channel 2 have similar values. By mapping these values, an image showing the presence of algae can be made. Such an image is seen in Fig. 5.3. The scale on the right is the value given by Eq. (5.1).

Also, this kind of ratio yields a dimensionless quantity, which means that all anomalies are suppressed, such as geometrical differences on the insulator, fluctuations of the laser intensity etc.

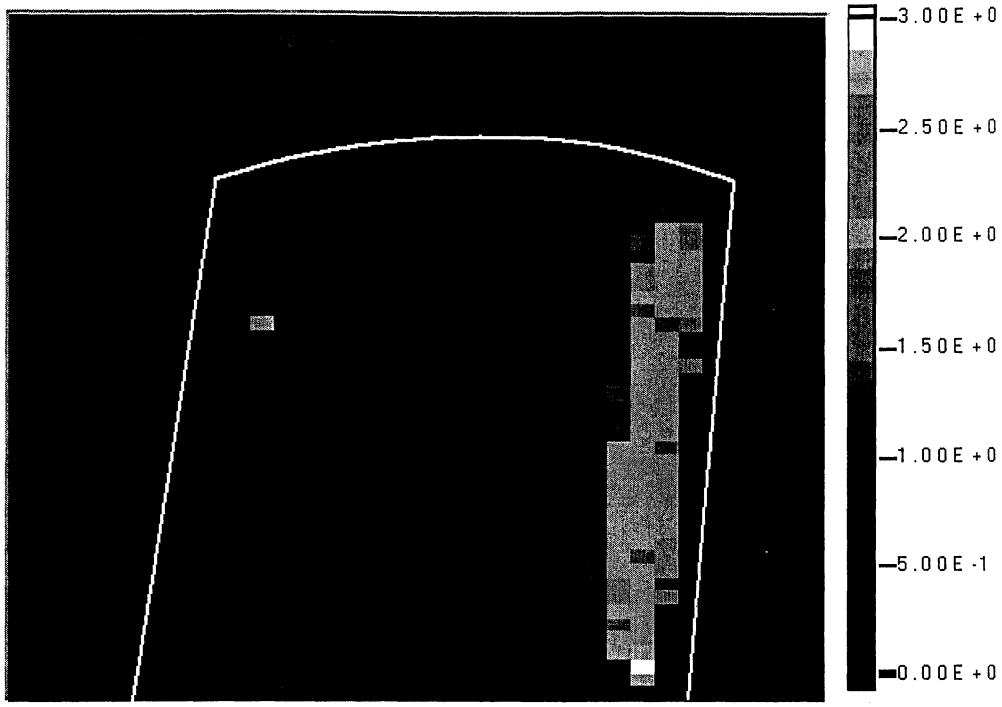

Figure 5.3 - A processed image showing the distribution of algal growth on an insulator. The line roughly marks the outline of the insulator.

These measurements led to a conference submission to CLEO Europe (European Conference on Lasers and Electro-Optics) in June 2003. The abstract, now accepted for oral presentation, is found in Appendix A. There was also a submission to ISH (International Symposium on High-Voltage Engineering) in August 2003. This paper is found in Appendix B. It also, in a more detailed way, describes the motivation for these types of measurements.

5.3.3 *Multivariate Analysis*

By using multivariate analysis to process the data, differences that cannot easily be found by inspection may be extracted. The theory of multivariate analysis is discussed in [21].

The idea of multivariate analysis, when trying to find particular characteristics of spectra, is to use principal component analysis (PCA) to change the coordinate system. The principal components (PC:s) are chosen so that PC1 represents the direction of greatest variance among the data. PC2 is then chosen orthogonal to PC1 along the direction of greatest variance among the remaining data. This means that in the new coordinate system, the data are uncorrelated.

Usually, the spectral data are similar to great extents, so the data can be well approximated using only a few of the PC axes. Certain properties that occur in spectra that are dissimilar from others will hopefully appear as an own PC, which makes it easy to distinguish these spectra.

5.4 Laser-Induced Breakdown Spectroscopy

5.4.1 *Set-up of the Measurements*

The theory of LIBS was briefly discussed in Sect. 2.3.4. The LIBS technique is a frequently used method for analysing materials, but it has not until recently been shown that it can be used at long range to study solid targets [5]. It was therefore of interest to find out if it was possible to gather LIBS spectra using our LIDAR system.

During the measurements made using the LIBS technique, tripled Nd:YAG laser radiation (355 nm) was used to excite the target material. To achieve breakdown in the material, the beam has to be focused onto a small point. Due to the set-up of the transmitter, it is not possible to achieve a small enough focus at the target. This is because the outgoing laser beam is no more than 3 cm in diameter. Due to the properties of Gaussian beams, a larger outgoing beam diameter makes a smaller focus possible to accomplish [11].

The radius of the beam is given by

$$w^2(z) = w_0^2\left[1+\left(\frac{z}{z_R}\right)^2\right], \tag{5.2}$$

where $w(z)$ is the radius of the beam at distance z from the beam waist. The beam waist is the point having smallest beam radius, w_0. z_R is the Rayleigh range and is defined as

$$z_R = \frac{\pi w_0^2}{\lambda}, \tag{5.3}$$

where λ is the wavelength of the light. Now, for distances z far away from the beam waist (i.e. where $z >> z_R$), Eq. (5.2) can be approximated by

$$w(z) \approx w_0 \frac{z}{z_R} = \frac{\lambda z}{\pi w_0}. \tag{5.4}$$

Rewriting Eq. (5.4) to find the beam waist diameter, knowing the beam diameter, $w(z)$, at range z we get

$$w_0 = \frac{\lambda z}{\pi w}. \tag{5.5}$$

Since we know the beam radius w = 1.5 cm at z = 60 m and λ = 355 nm we can put these values into the equation and we find that w_0 = 0.45 mm. This would, in fact, be a sufficiently small focus, but in reality the smallest focus achieved had a 4-mm radius, which is not enough to achieve breakdown in the material. The difference between theory and reality is because the laser transmits light that is not a perfect Gaussian beam.

Just to check that the approximation was valid, we can calculate the Rayleigh range z_R and compare it with the range z. Putting our values into

Eq. (5.3) we get z_R = 1.8 m which is much smaller than 60 m and thus our approximation was all right.

To overcome this problem and still be able to study important aspects of remote LIBS, a 50-cm focal length lens was placed in front of the target. However, this would not be needed with a slight rebuilding of the transmitter, to be discussed below.

The backscattered light is collected using the same OMA system (as described in Sect. 3.4.1). The OMA system is time-gated, to that the interesting signal is not disappearing in background light, and the signal is averaged over a number of shots to improve the signal-to-noise ratio. An evident fluorescence signal can also be found, making it more difficult to find the LIBS signal, but the latter signal is delayed in time with respect to the first one. This means that the LIBS signal is found by increasing the delay of the time-gate on the OMA system (by a few hundred ns).

5.4.2 Results

A number of different materials were studied and a few of the gathered spectra are seen in the figures below. Fig. 5.4 shows the LIBS spectrum from copper, Fig. 5.5 shows the LIBS spectrum from zinc and Fig. 5.6 the LIBS spectrum from brass, which is an alloy of zinc and copper. When comparing these spectra it is easily seen which peaks in the brass come from copper and which come from zinc.

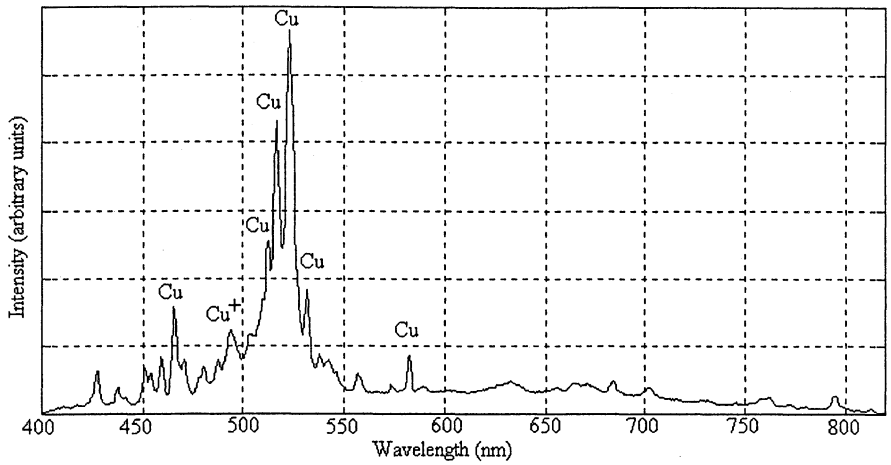

Figure 5.4 - LIBS spectrum from copper (Cu).

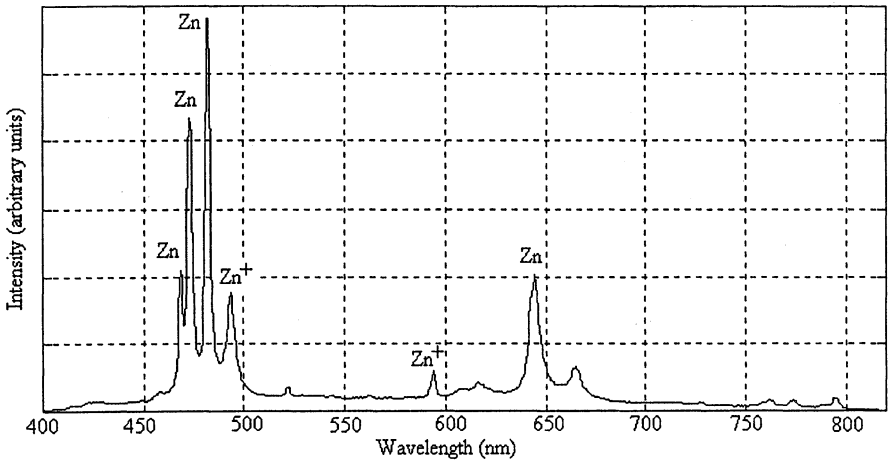

Figure 5.5 - LIBS spectrum from zinc (Zn).

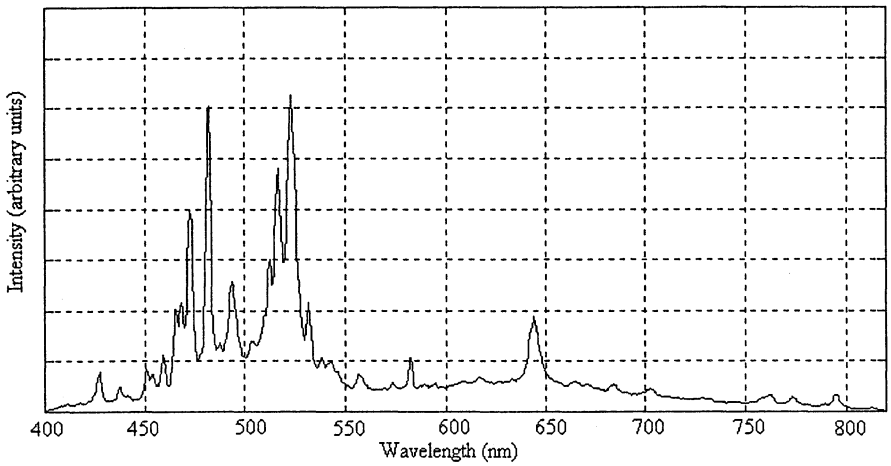

Figure 5.6 - LIBS spectrum from brass, an alloy of Zn and Cu.

In Fig. 5.4 and Fig. 5.5, the sharpest peaks have been identified. The peak data is taken from [22].

This is just an example of what kind of spectra can be achieved using the LIBS method. The main objective of these measurements was to find out whether it was at all possible to get results.

Studies were also made to examine the importance of the delay between firing the laser and the time-gate on the OMA system. The result of the study is seen in Fig. 5.7, where a piece of Aluminium has been examined. Each part of the figure represents a different delay on the time-gate and each spectrum has been gathered by taking the average over 200 shots. In Fig. 5.7, a) shows the first detected signal, b) is delayed 100 ns, c) 300 ns, d) 500 ns, e) 3.2 μs and f) is delayed 19.4 μs.

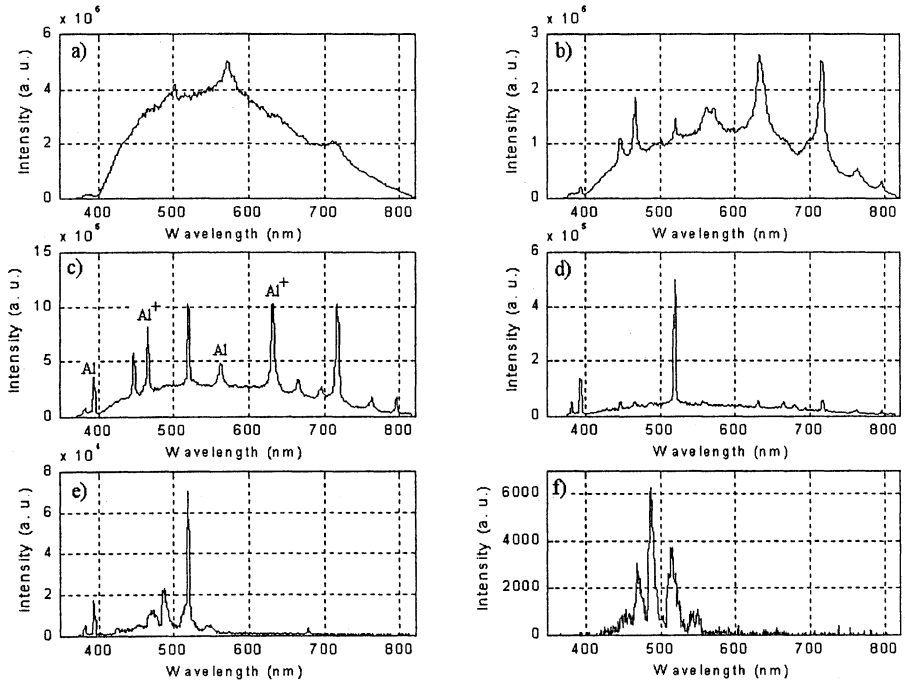

Figure 5.7 - Development of the LIBS spectrum as the time delay is increased.

As can be seen in Fig. 5.7a, the first light arriving to the detector is dominated by intense white-light radiation, but a few of the representative peaks can already be made out. As the delay is increased by 100 ns, the white-light radiation is reduced and the peaks start to become prominent as seen in Fig. 5.7b. If the delay is increased another 200 ns (Fig. 5.7c), there is still some white-light radiation, but the peaks are easily isolated. This is the delay that was used when other spectra were taken. In this part, a few peaks are indicated [23]. It can be seen that the ionic lines are seen only at early times. This is because ions are created in the plasma, but will swiftly recombine so that only the atomic lines are present at later times.

As the delay is further increased, to 500 ns in Fig. 5.7d, some of the peaks start to disappear, whereas some are still prominent. At much later times, as in Fig. 5.7e, where the delay is 3.2 μs, a few of the peaks still remain, whereas most of the peaks are not seen. Note also that the total intensity is decreased as the delay is increased. At this time a few other peaks can be

seen, however, these are probably not a part of the LIBS signal. Most likely is that they appear at all times, but not until now is the other radiation weak enough for them to be seen. Finally at very long delay times, 19.4 μs, as seen in Fig. 5.7f, no LIBS signal can be seen any more.

Moreover, a test was done to find how the signal depends on how close to focus the material is placed, but these results are yet to be analysed.

5.4.3 *New Design*

The main problem with the LIDAR system for making LIBS measurements is that it is not possible to get the laser spot small enough on the target, as discussed in Sect. 5.4.1. A solution to this problem would be to enlarge the beam diameter out of the system and thus be able to achieve a smaller focus. This could be done by sending the beam out using the large spherical mirror that is used to gather the incoming light. The new design is shown in Fig. 5.8.

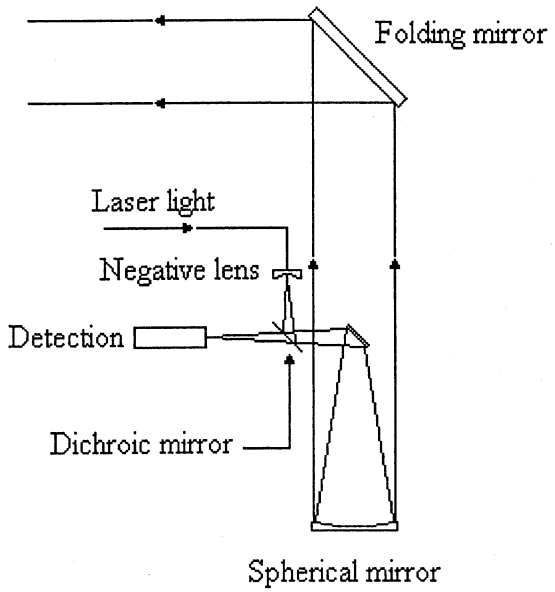

Figure 5.8 - The planned new design of the transmitter.

The detection stage, as shown in Fig. 3.4, does not need to be altered. The dichroic mirror links the 355-nm outgoing light into the telescope while the backscattered light is transmitted to the detector.

Using this design, the outgoing beam radius would be as much as 20 cm which, using Eq. (5.5), would give a theoretical radius at focus of 34 μm at a distance of 60 m. Assuming that the practical beam radius would be about 10 times greater (as it was in the old design) the focus would be about 0.4 mm which should be enough to achieve breakdown.

6 Conclusions and Future Work

Within this project, three different aspects have been focused on. First, the existing calibration unit has been redesigned to improve its performance. The old design did not work for all kinds of measurements that are otherwise possible. The obvious continuation is to actually perform the alterations of it, so far the design has been done, but is yet to be built. Also, the unit needs to be tested, to see that it works properly in all wavelength regions.

Further, LIF measurements on electrical insulators have been performed. Studies to find algal growth on buildings had previously been performed and this study used the same technique. The study was made to make sure that it is possible to make this kind of measurements on insulators, in a real-life situation. Good results were extracted from these measurements, showing that algae detection on electrical insulators can be performed. This project will be continued and more measurements will be made, aiming at monitoring fungal growth on the insulators. This is a greater challenge, since fungus does not have the easily found chlorophyll peak.

Finally, measurements using the LIBS technique have been performed, as a test to find out whether it is possible to use our LIDAR system for these kinds of studies. The results were very promising. However, it turned out that the system needs to be slightly rebuilt. The next step is naturally to make these alterations to the system and to perform tests to fully explore the potential of remote LIBS.

7 Acknowledgements

This project has been carried out at the Atomic Physics Division of the Lund Institute of Technology as a thesis for the degree of Master of Science.

Of course, I could not have done this without help and I would like to thank my supervisor Sune Svanberg for taking me on, for his endless enthusiasm and for all his assistance.

Also, I would like to thank Hans Edner for all help, especially during the measurements and Petter Weibring for taking care of me and introducing me to the many complex aspects of the LIDAR system.

Furthermore, I would like to thank Magnus Bengtsson, Mikael Sjöholm, Andreas Dernfalk and Gabriel Somesfalean for all help during the measurements and for the fun times in the lab.

Lastly, I would like to thank everybody else helping me in my work and everyone at the Atomic Physics Division for making me feel welcome.

8 List of Acronyms

BBO	β-Barium BOrate (crystal)
CCD	Charge Coupled Device
DIAL	DIfferential Absorption LIDAR
HeNe	Helium-Neon
IR	InfraRed
LIBS	Laser Induced Breakdown Spectroscopy
LIDAR	LIght Detection And Ranging
LIF	Laser Induced Fluorescence
LIPS	Laser Induced Plasma Spectrometry
NA	Numerical Aperture
Nd	Neodymium
OMA	Optical Multi-channel Analyser
OPA	Optical Parametric Amplifier
OPO	Optical Parametric Oscillator
PC	Principal Component
PCA	Principal Component Analysis
PMT	PhotoMultiplier Tube
UV	UltraViolet
YAG	Yttrium Aluminium Garnet

9 References

[1] Sune Svanberg, *Atomic and Molecular Spectroscopy - Basic Aspects and Practical Applications* (Springer-Verlag, Lund, 2001).

[2] Petter Weibring, *Environmental Monitoring by Multi-Spectral Lidar Techniques*, PhD Thesis, Lund Reports on Atomic Physics, LRAP-284 (Lund, July 2002).

[3] P. Weibring, Th. Johansson, H. Edner, S. Svanberg, B. Sundnér, V. Raimondi, G. Cecchi and L. Pantani, *Fluorescence Lidar Imaging of Historical Monuments*, *Applied Optics* **40**, 6111 (2001).

[4] D. Lognoli, G. Cecchi, I. Mochi, L. Pantani, V. Raimondi, R. Chiari, Th. Johansson, P. Weibring, H. Edner and S. Svanberg, *Fluorescence Lidar Imaging of the Parma Cathedral and Baptistery*, *Applied Physics B*, in press (2003).

[5] S. Palanco, J. M. Baena and J. J. Laserna, *Open-path laser-induced plasma spectrometry for remote analytical measurements on solid surfaces, Spectrochimica Acta Part B* **57** (2002) 591-599.

[6] H. Cormican, *Laser-Induced Breakdown Spectroscopy*, http://www.andor-tech.com/Japan/libs.html

[7] Spectra Physics Inc., *Quanta-Ray MOPO-730 Optical Parametric Oscillator Instruction Manual* (January 1995).

[8] R. W. Boyd, *Non-linear Optics* (Academic Press, San Diego, 1992).

[9] P. Weibring, H. Edner and S. Svanberg, *Versatile Mobile Lidar System for Environmental Monitoring*, Submitted to *Applied Optics*, July (2002).

[10] P. Weibring, J.N. Smith, H. Edner and S. Svanberg, *Development and Testing of a Frequency Agile Optical Parametric Oscillator System for Differential Absorption Lidar*, Submitted to *Review of Scientific Instruments*, July (2002).

[11] O. Svelto, *Principles of Lasers* (Plenum Press, New York, 4th edition 1998).

[12] C. af Klinteberg, M. Andreasson, O. Sandström, S. Andersson-Engels and S. Svanberg, *Compact medical fluorosensor for minimally invasive tissue characterisation*, *Rev. Sci. Instr.*, to appear.

[13] National Instruments, *LabView Users Manual*, http://www.ni.com/pdf/manuals/320999b.pdf

[14] Fabian Mellegård, *Development and construction of an automatic calibration unit for a differential absorption LIDAR system*, Master Thesis, Lund Reports on Atomic Physics, LRAP-264 (Lund, October 2000).

[15] Thorlabs Inc., Catalogue, Volume 15, (2003), p. 421, 426.

[16] P. Weibring, M. Andersson, H. Edner and S. Svanberg, *Remote Monitoring of Industrial Emissions by Combination of Lidar and Plume Velocity Measurements*, *Applied Physics B* **66**, 383 (1998).

[17] P. Weibring, H. Edner, S. Svanberg, G. Cecchi, L. Pantani, R. Ferrara and T. Caltabiano, *Monitoring of Volcanic Sulphur Dioxide Emissions using Differential Absorption Lidar (DIAL), Differential Optical Absorption Spectroscopy (DOAS) and Correlation Spectroscopy (COSPEC)*, *Applied Physics B* **67**, 419 (1998).

[18] P. Weibring, J. Swartling, H. Edner, S. Svanberg, T. Caltabiano, D. Condarelli, G. Cecchi and L. Pantani, *Optical Monitoring of Volcanic Sulphur Dioxide Emissions - Comparison Between Four Different Remote-sensing Spectroscopic Techniques*, *Optics and Lasers in Engineering* **37**, 267 (2002).

[19] I. Wängberg, H. Edner, R. Ferrara, E. Lanzillotta, J. Munthe, J. Sommar, S. Svanberg, M. Sjöholm and P. Weibring, *Mercury Emissions from a Chlor-alkali Plant in Sweden*, *The Science of the Total Environment*, in press (2003).

[20] S. Svanberg, *Multi-Spectral Imaging - from Astronomy to Microscopy - from Radiowaves to Gammarays*, (Lund, October 2001).

[21] K. H. Esbensen, D. Guyot, F. Westad and L. P. Houmøller, *Multivariate Data Analysis - in Practice*, (CAMO, Oslo, 5th edition 2002).

[22] David R. Lide, *CRC Handbook of Chemistry and Physics*, (CRC Press, 74th edition 1993).

[23] A. R. Striganov and N. S. Sventitskii, *Tables of Spectral Lines and Ionized Atoms*, (Plenum Data Corporation, New York, 1968).

Appendices

Appendix A

Lidar fluorescence measurements of algal growth on electrical insulators

Magnus Bengtsson, Rasmus Grönlund, Mikael Sjöholm, Petter Weibring, Stefan Kröll, Hans Edner, Sune Svanberg,
Atomic Physics Division, Lund Institute of Technology, P.O. Box 118, S-221 00 Lund, Sweden, and
Andreas Dernfalk,
Department of Electric Power Engineering, Chalmers University of Technology, S-412 96 Göteborg, Sweden

Fluorescence measurements using lidar techniques have been shown to be useful for monitoring of algal growth on e.g. historical monuments [1]. In this experiment similar measurements were performed on electrical insulators to examine the correlation between algal growth and the quality of the insulator, a factor of importance in the high-voltage grid management.

The measurements were performed using the lidar system of the Lund Institute of Technology [2]. A 20 Hz pulsed 355 nm Nd:YAG laser was used to induce fluorescence on the insulator and the beam was scanned in steps of approximately 4 cm across the area of the insulator, which was placed at a distance of 60 m. The fluorescence signal was detected using a time-gated optical multi-channel analyser system. The algal growth can easily be detected from the 690 nm chlorophyll fluorescence peak.

The spectrum in each point on the insulator is registered. A typical spectrum showing algal growth is seen in figure 1 below. The vertical lines mark three different wavelength bands.

By calculating the average signal in each wavelength band and evaluating a function of these values, different properties of the spectrum can be enhanced. In this case, where it is of interest to detect any occurrence of algal growth, a good function would be: $\frac{\text{channel 3} - \text{channel 2}}{\text{channel 1}}$, where the different channels are defined as in figure 1.

In this way, only the points containing a large peak at 690 nm will give a large value. By mapping these values, a picture showing the presence of algae can be made. Such a picture is seen in figure 2. In the picture, each pixel corresponds to an area of approximately 3×5 cm. The line marks the approximate outline of the insulator and the scale to the right is the value given by the equation above.

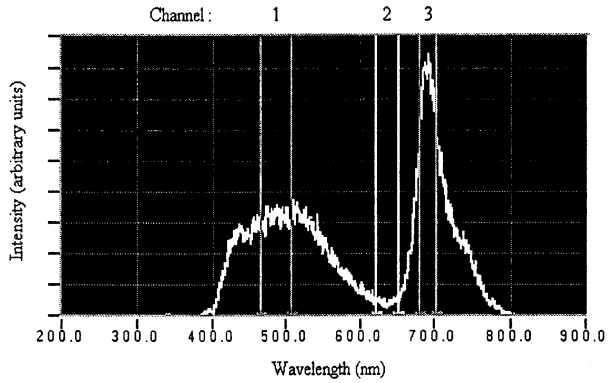

Figure 1 - A typical fluorescence spectrum from a part of the insulator covered by algae.

Figure 2 - A processed image showing the distribution of algal growth on the insulator.

References

1. P. Weibring, Th. Johansson, H. Edner, S. Svanberg, B. Sundnér, V. Raimondi, G. Cecchi and L. Pantani, Fluorescence lidar imaging of historical monuments, *Applied Optics* **40**, 6111 (2001).
2. P. Weibring, H. Edner and S. Svanberg, Versatile Mobile Lidar System for Environmental Monitoring, Submitted to *Applied Optics*, July (2002).

Appendix B

Laser-induced fluorescence spectroscopy for detection of biological contamination on composite insulators

A.D. Dernfalk[1], M. Bengtsson[2], R. Grönlund[2], M. Sjöholm[2], P. Weibring[2], H. Edner[2], S.M. Gubanski[1], S. Kröll[2] and S. Svanberg[2]
[1]Chalmers University of Technology, Gothenburg, Sweden
[2]Lund Institute of Technology, Lund, Sweden

Abstract: A new technique for remote detection of biological contamination on high-voltage outdoor insulators has been investigated. The technique, which is based on laser-induced fluorescence (LIF) spectroscopy, has been applied to study surfaces of real silicon rubber insulators from a distance of approximately 60 m. Measurements were performed outdoors on a number of clean, as well as, biologically contaminated insulators. Several types of biological contamination were included, as five of the studied insulators had become covered when installed in Sweden, and another three had been contaminated by fungal growth in laboratory. Fluorescence spectra obtained from the surfaces of the described insulators are presented and the applicability of the technique is discussed and compared with photographic methods.

1. Introduction

Reports on biological growth on outdoor insulators reveal that microbiological colonization of ceramic as well as composite insulators can take place in all parts of the world [1-14]. Since the impact of biological growth on insulator performance is not fully understood, it makes utility engineers concerned [14, 15]. The fact that microorganisms grow on composite insulators is of special concern. Silicone rubbers are known to exhibit high resistance to biological degradation. One of the reasons is that the material consists of both organic as well as inorganic components, and that microorganisms like fungi cannot digest the inorganic parts [16]. However, it is believed that in service, composite insulators are mostly attacked by fungi [8, 17].

There is a number of reports on biological contamination of composite insulators [1, 2, 4-13, 15, 18], about half of them from tropical climate [2, 6-8, 11, 15, 18]. Different types of silicon rubber (SIR) insulators, epoxies and blends of silicone and ethylene-propylene-diene monomer rubber (EPDM) have been found to support growth of bacteria, algae, fungi and lichen. However, so far there is not much information published on the growth on EPDM insulators.

This study is a step in a process of investigating the influence of biological growth on insulator performance. More specifically, the aim is to develop a method that can be used to remotely detect and measure/characterize growth and growth distributions.

At close distance, presence of for instance algae on an insulator surface can be detected through visual inspection. However, in order to get a measure of its "severity", more refined techniques have to be used. An example of such a diagnostic technique is photography followed by digital image analysis, which has been proposed by one of the authors [19, 20]. Using this technique, it is possible to get measures of area covered by the growth and its distribution. However, it is difficult to differentiate between regions covered by microorganisms and regions covered by other contamination.

The technique investigated in this study, laser-induced fluorescence (LIF) spectroscopy, has e.g. been utilized for imaging of historical monuments [21] and previously been suggested for insulator diagnostics [22]. In the latter report, the authors presented fluorescence spectra obtained in laboratory from different SIR and EPDM materials and from SIR surfaces where its hydrophobic properties had been reduced through water immersion. In the present study, LIF spectra have been obtained from real insulators partly covered by biological growth using a mobile measuring system. To simulate a real situation, i.e. studying insulators installed in a HV-system, measurements were performed outdoors at a distance of about 60 m.

2. Experimental set-up

The used mobile LIght Detection And Ranging (LIDAR) system, housed in a Volvo F610 truck, is based on all solid-state laser technology, and can be used for multi-wavelength excitation and detection in fluorescence imaging, gas concentration- and flux measurements [23]. The system is self-contained, with a diesel powered electrical generator, making it well-suited for field measurements.

In the present experiment, only a part of the laser system, a frequency tripled Nd:YAG laser (Quanta-Ray) was used. This laser delivers pulses with a duration of 4-5 ns at a repetition rate of 20 Hz and a wavelength of 355 nm. The laser beam is passed through an aperture to produce a better mode, rendering a beam diameter of 5 mm and a pulse energy

of around 25 mJ. After a totally reflecting 90 degree prism, the laser beam is expanded in a vertically mounted Galilean quartz telescope to 3 cm in diameter. This gives sufficiently low laser intensity on the computer controlled output folding mirror mounted in a dome, Figure 1, not to damage the mirror. The transmitted excitation light is directed towards a remote target, which in the present work was a number of insulators.

From a control computer, the dome can be rotated 360 degrees (resolution of 0.0035 degrees) with a stepper motor in the azimuthal angle and the folding mirror can be tilted from –10 to +55 degrees (resolution of 0.011 degrees) in the polar angle. At the target located 60 m from the laser source, this corresponds to a resolution of 3.7 mm and 12 mm respectively. However, if using this resolution the time for acquiring spectra from the complete insulator surface would be very long. Therefore, a beam diameter of ~20 mm and a separation between adjacent measurement points of ~20 mm at the insulator were used. The change of position of the laser beam at the target due to mechanical instability of the whole truck was estimated to 5 mm.

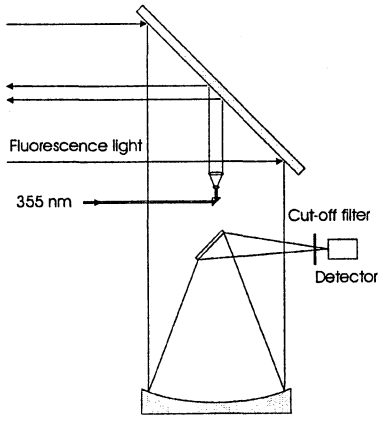

Figure 1. Dome and light receiving unit.

The remotely emitted fluorescence light is received by a 40 cm diameter Newtonian telescope (f=1 m), coaxially mounted with the Galilean telescope. By using a cut-off filter in front of the focus of the telescope, the excitation light is discriminated. An optical fibre, 600 μm core diameter and numerical aperture 0.22, guides the fluorescence light to a compact time-gated Optical Multi-channel Analyser system (OMA) designed for medical use. It consists of a spectrometer and a charge coupled device (CCD) camera. In the OMA system a beamsplitter and a cut-off filter selects only wavelengths longer than approximately 385 nm, effectively suppressing the dominating excitation light which is still of appreciable intensity.

A crossed Czerny-Turner spectrograph diffracts the fluorescence light to the image intensified CCD. The thermo-electrically cooled detector has a CCD array with 1024x128 pixels where the 128 pixels are binned. The resulting resolution for the OMA system, set by the slit width (100 μm), is 2.2 nm up to 805 nm. Ambient daylight is suppressed by using a time-gate of 100 ns, positioned in time by a properly delayed trigger signal from the laser. Spectra from the OMA system are acquired by a data collection computer that stores the spectrum together with information about the measurement coordinates.

Studied insulators

The present study included eight insulators partly covered by biological contamination and one clean reference insulator. The insulators have been divided into three categories, A-C, according to their design. Type A and B are of line suspension type, while insulators of type C are of apparatus type and have a hollow core. All insulators have sheds and sheath of SIR. However, the formulation differs between the three categories.

The three insulators A have been installed in a 10 kV distribution system in Sweden for approximately 12 years, where they have become covered by a rather thick green growth. However, at the time of the measurement, the growth had turned brown/grey, as the insulators had been kept in laboratory for 6 months. Three of the four insulators B had been exposed to fungal spores and kept in a climate chamber for approximately two years [19]. This treatment lead to colonisation of the insulator surfaces by fungi in spot-like manner. The insulators of the third type, C, have been installed in a test station 30 km south of Gothenburg, Sweden, since 1995. They had become covered by a greenish growth on the surfaces shaded from direct sunlight.

During the measurements, the insulators were placed about 60 m away from the truck. To get a better view of the growth, which mainly were located on the upper side of the sheds, the insulators had to be turned up-side-down, tilting away from the point of observation. The insulators C were supported by a wooden structure, and tilted an angle of 30 degrees. Type A and B were fixed using horizontal metal rods and tilted 60 and 50 degrees, respectively. As a safety precaution, a board covered with black paper was put behind the insulators, hindering the laser beam to propagate further.

3. Results

LIF spectra were obtained from characteristic points on the insulators. A typical region with thick, green growth located on a shed of one of insulators C gave the spectrum shown in Figure 2. As seen, there is a large peak located around 680-690 nm, corresponding to the well-known fluorescence peak of chlorophyll *a* at 685 nm [23]. Further, the shoulder on the right probably corresponds to another smaller fluorescence peak of chlorophyll at 735 nm.

Comparison of the obtained spectra gave that the fluorescence peak of chlorophyll around 685 nm is significant for the region covered by growth. The parts

of the insulator, which are not covered by algae, show a low and decaying fluorescence above 600 nm. The spectra obtained from measurements on insulators of type B were more difficult to interpret due to several reasons. First, these insulators were covered by fungi, which do not utilize photosynthesis, and thus not contain any chlorophyll. Second, the growth was more or less evenly distributed over the surface in the form of small isolated spots. As the spatial resolution of the measurements was in the order of 20 mm, spectra could not be obtained from regions completely without growth or regions totally covered by growth. However, comparison of typical spectra from a clean reference insulator and from insulators with growth shows that the total fluorescence of the contaminated insulator is lower, compared to the clean insulator, Figure 3. Further, if the amplitudes are normalized, it is revealed that the contaminated insulator has a slightly higher relative fluorescence in the wavelength band 520-600 nm.

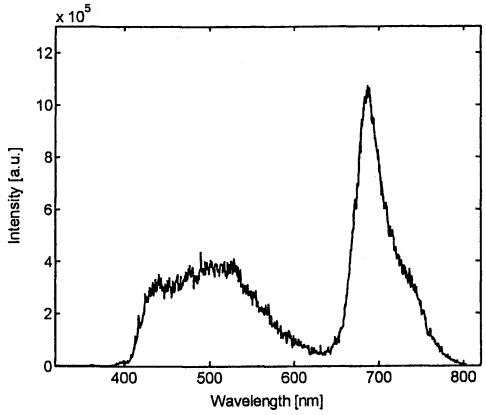

Figure 2. Typical spectra obtained from a region with green growth on one of the insulators C.

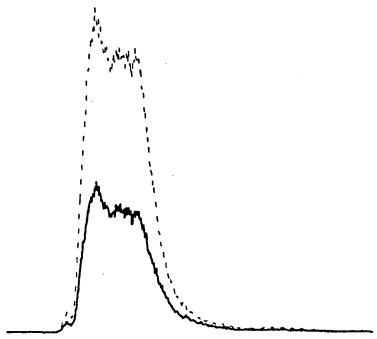

Figure 3. Spectra from clean reference insulator B (dashed) and an insulator B with growth (solid).

Measurements on insulators A revealed that these had a low fluorescence compared to the other insulators studied. As the insulators of type B, the intensity of fluoresced light was much lower from regions covered by growth, than from clean regions, Figure 4. Further, regions covered by growth showed an increased fluorescence in an interval around 685 nm. However, the difference was very small compared to the insulators of type C. The reason for the low response was probably that the algae had died, due to desiccation and lack of sun radiation, when stored in laboratory.

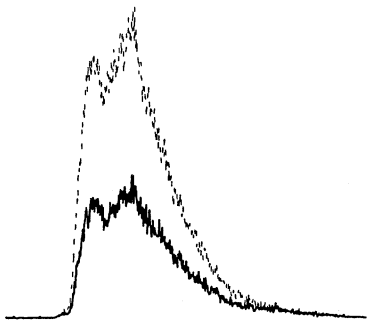

Figure 4. Spectra from a region covered by growth (solid) and a region without visible growth (dashed), on one of the type A insulators.

As the aim was to study distributions of biological contamination, the dome was programmed to scan a window covering a substantial part of the insulator surface. The data were presented as gray level images where the intensity was proportional to the intensity of the fluorescence light within a specific wavelength band. The result of a scan of one of the insulators C is presented in Figure 5, together with a photograph (left) taken from the roof of the truck using a system camera equipped with a 300 mm telephoto lens. In the center image, depicting the average overall fluorescence intensity, it can be seen that the supporting wooden structure has a strong fluorescence (black) compared to the other materials present. However, when only studying the fluorescence peak of chlorophyll, i.e. the intensity in a range from 670-700 nm, the chlorophyll becomes clearly visible (right). As stated above, this is interpreted as presence of algae cells on the surface of the insulator.

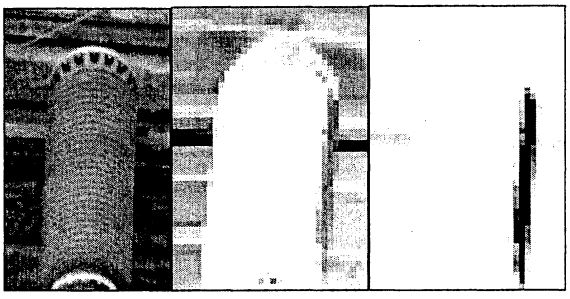

Figure 5. Type C insulator with algae on the right side. Left to right: Photograph, mean intensity in 400-800 nm band and in 670-700 nm band.

In order to improve sensitivity and avoid incorrect classification of regions, the obtained spectral data were processed. Average intensities were calculated for two different wavelength bands, B_1 and B_2, and the intensity ratio $I(B_2)/I(B_1)$ were formed. The main advantage of these types of dimensionless ratios is that they eliminate the influence of geometrical artifacts, i.e. intensity differences due to different directions of

studied surfaces [21]. An example is shown in Figure 6. Image a) shows a photograph taken from close distance, b) shows the average fluorescence intensity in the 410-500 nm band, while c) shows the average intensity in the 670-690 nm band. The ratio of the light fluoresced in the two bands is shown in d), where the dark areas are well corresponding to the regions covered by green growth.

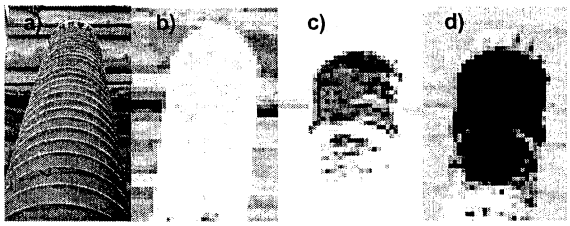

Figure 6. a) Photograph of an insulator of type C, b) average intensity in 410-500 nm band, c) in 670-690 nm band and d) ratio of intensities in 670-690 nm band and 410-500 nm band.

4. Discussion and Conclusions

In comparison with photography, LIF can be used to get a higher sensitivity, especially when there is a large difference in fluorescence between insulator material and contamination. Further, as collection of fluorescence light only is performed under a short period of time, ~100 ns, measurements are not affected by sun radiation.

Comparison of the obtained spectra shows that the fluorescence peak of chlorophyll around 685 nm is significant for the regions covered by algae, while regions with no algae showed low fluorescence in the same wavelength interval. Presence of growth without chlorophyll, i.e. fungi and bacteria, did only cause small changes in the shape of the spectra, compared to the ones of clean surfaces. The most apparent difference here was an amplitude reduction. However, it is not unlikely that a good detection sensitivity of growth without chlorophyll can be obtained using other excitation wavelengths and more extensive data analysis. In conclusion, it has been shown that remote LIF measurements can be used to detect and measure distribution of biological contamination on composite insulators.

5. References

[1] K. Kunde, R. Hennings, M. Kuhl, A. Schütz, H. Jansses, and U. Stietzal, "New experience with composite insulators", Cigré, Paper No. 15-206, 1998

[2] M. A. R. M. Fernando, "Performance of non-ceramic insulators in tropical environments", Ph.D. Thesis, Chalmers University of Technology, Goteborg, Sweden, 1999

[3] R. D. McAfee, R. D. Heaton, J. M. King, and A. U. Falster, "A study of biological contaminants on HV porcelain insulators", *Electric Power System Research*, Vol. 42, No. 1, pp. 35-39, July, 1997

[4] G. B. Rackliffe, R. E. Lee, D. E. Fritz, and R. W. Harmon, "Performance evaluation of 15-kV polymeric insulators for dead-end type applications on distribution systems", *IEEE Trans. on P. D.*, Vol. 4, No. 2, pp. 1223-1231, April, 1989

[5] I. Gutman, R. Hartings, and W. L. Vosloo, "Field testing of composite insulators at natural test stations in South Africa", 11th ISH, London, UK, pp. 50-53, 1999

[6] M. A. R. M. Fernando and S. M. Gubanski, "Performance of nonceramic insulators under tropical field conditions", *IEEE Trans on P. D.*, Vol. 15, No. 1, pp. 355-360, January, 2000

[7] S. M. Gubanski, M. A. R. M. Fernando, S. J. Pietr, J. Matula, and A. Kyaruzi, "Effects of biological contamination on insulator performance", Proceedings of the 6th Int. Conf. on Properties and Applications of Dielectric Materials, Xi'an, China, pp. 797-801, 2000

[8] Research findings comparing performance of different insulator designs on distribution lines in tropical environments", INMR, Vol. 7, No. 6, pp. 46-53, 1999

[9] Research at Chalmers focusing and promoting developments in outdoor electrical insulation", INMR, Vol. 8, No. 2, pp. 28-36, 2000

[10] Growing interest at Entergy to assess techniques for in service monitoring of composite insulators", INMR, Vol. 7, No. 2, pp. 30-34, 1999

[11] R. S. Gorur, J. Montesinos, R. Roberson, J. Burnham, and R. Hill, "Mold growth on nonceramic insulators and its impact on electrical performance", IEEE Transmission and Distribution Conf., New Orleans, USA, pp. 818-822, 1999

[12] R. S. Gorur and B. S. Bernstein, "Field and laboratory aging of polymeric distribution cable terminations. I. Field aging", *IEEE Trans. on P. D.*, Vol. 13, No. 2, pp. 316-322, 1998

[13] M. Josho, H. Miyakawa, M. Sakata, K. Arakawa, K. Tsuge, D. Usami, T. Kondo, and Y. Utsumi, "Long term field test of polymer insulators at the Yonezawa Test Site", IEEJ Trans. on HV, Paper No. HV-01-72, 2001

[14] F. Coowar and P. R. P. Hoole, "Discharge characteristics of alga-contaminated string insulators in the tropics", *Electric Power System Research*, Vol. 5, No. 3, pp. 215-218, 1988

[15] Experience with non-ceramic bushings at Florida-based utility", INMR, Vol. 5, No. 6, pp. 30-35, 1997

[16] A. Wolf, "Mould fungus growth on sanitary sealants", *Constr. and building materials*, Vol. 3, pp. 145-151, 1998

[17] F. Schmuck and R. Bärsch, "Electrochemical and microbiological phenomena during accelerated ageing tests of polymeric insulators", 8th ISH, Yokohama, Japan, Paper No. 41.02, 1993

[18] M. A. Mbwana, "Laboratory and field performance of polymeric insulators and RTV coatings", Lic. Thesis, Royal Institute of Technology, Stockholm, Sweden, 1997

[19] A. Dernfalk, "Image analysis for diagnostics of insulators with biological contamination", Lic. Thesis, Chalmers University of Technology, Gothenburg, Sweden, 2002

[20] A. Dernfalk and S. M. Gubanski, "Use of digital image analysis for studying biological contamination on nonceramic insulators", 12th ISH, Bangalore, India, pp. 599-602, 2001

[21] P. Weibring, T. Johansson, H. Edner, S. Svanberg, B. Sundnér, V. Raimondi, G. Cecchi, and L. Pantani, "Fluorescence lidar imaging of historical monumnets", *Applied Optics*, Vol. 40, No. 33, pp. 6111-6120, 2001

[22] A. Larsson, S. Kröll, A. D. Dernfalk, and S. M. Gubanski, "In-situ diagnostics of high-voltage insulation using laser-induced fluorescence spectroscopy", *IEEE Trans. on Dielectrics and Electrical Insul*, Vol. 9, pp. 274-281, 2002

[23] P. Weibring, "Environmental Monitoring by Multi-Spectral Lidar Techniques", Ph.D. Thesis, Lund Institute of Technology, Lund, Sweden, 2002

Author address: Andreas Dernfalk, Department of Electrical Engineering, Chalmers University of Technology, 412 96 Goteborg, Sweden. Email: andreas.dernfalk@elteknik.chalmers.se